SMART HEATING OF RESIDENTIAL SECTOR USING HEATING PANELS

Zhanar Rakhimbayeva, B.Eng

Submitted in fulfillment of the requirements
for the degree of Master of Science
in Mechanical & Aerospace Engineering

NAZARBAYEV UNIVERSITY

School of Engineering and Digital Sciences
Department of Mechanical & Aerospace Engineering
Nazarbayev University

53 Kabanbay Batyr Avenue,
Nur-Sultan city, Kazakhstan, 010000

Supervisor: Prof. Luis R. Rojas-Solórzano
Co-supervisor: Prof. Desmond Adair

December 2021

DECLARATION

I hereby, declare that this manuscript, entitled “Smart Heating of residential sector using heating panels”, is the result of my own work except for quotations and citations, which have been duly acknowledged.

I also declare that, to the best of my knowledge and belief, it has not been previously or concurrently submitted, in whole or in part, for any other degree or diploma at Nazarbayev University or any other national or intentional institution.

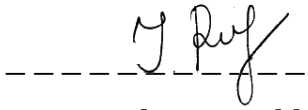

Name: Zhanar Rakhimbayeva

Date: 13.12.2021

Abstract

The motivation for this thesis lies in the problem of global warming that people are facing nowadays. Due to human activities through the burning of fossil fuels resulting in air pollution and greenhouse gas emissions, the temperature continues to rise and is expected to increase by another 2.4°C by the year 2050. To prevent this problem, people are now focusing on reducing energy consumption as it uses fossil fuels. The residential sector is one of the largest energy consumers, especially for space heating, as people spend most of their lives indoors. Therefore, this thesis presents a new approach for space heating with occupants. The main idea is to design a focused heating panel placed on the ceiling at a reasonable distance from the occupant's head. This heating system directly heats only the occupant and not the rest of the environment in the room.

In this numerical study, the CFD simulation was implemented with a manikin to analyze the performance of two different systems on the occupant under winter conditions. The experimental data and the setup model were adopted from the research study for the benchmark scenario. After achieving good performance in discretizing the model, three scenarios with heating systems were used. The main parameter to be achieved in all three cases was Predicted Mean Vote (PMV) and Predicted Percentage Dissatisfied (PPD) to create a comfortable environment in the room. All scenarios with the heating system complied with ASHRAE Standard 55-2017 and ISO 7730, except for case 1 with the ventilation system. However, the conventional type of space heating was 6.9% more energy efficient than the proposed heating approach.

Acknowledgements

I would like to express my sincere gratitude to Prof. Luiz Rojas, my supervisor, whose encouragement and constant support I will never forget throughout the study period. I am grateful that I was accepted as your student and that you continued to believe in me throughout the last two years. I am grateful to you for guiding me from the beginning of research to the end and helping me to understand my work better.

I would also like to thank the members of the school committee and my groupmates who have always supported and guided me.

Table of Contents

List of Abbreviations & Symbols

$\bar{t}_r$	Mean radiant temperature
$\dot{h}$	Static enthalpy
h_c	Convective heat transfer coefficient
I_{cl}	Clothing insulation
$\dot{Q}$	Heat flux
$\vec{f}$	Body forces
f_{cl}	Clothing surface area factor
$\dot{m}$	Mass flow at inlet
p_a	Water vapor partial pressure
$\dot{q}$	Heat transfer
t_a	Air temperature
t_{cl}	Clothing surface temperature
v_{ar}	Relative air velocity
ε_v	Spectral emissivity
∇	Gradient vector operator
3D	Three-dimensional
ASHRAE	American Society of Heating, Refrigerating and Air Conditioning Engineers
CFD	Computational Fluid Dynamics
CTM	Computational Thermal Manikin
CTM	Computational Thermal Manikin
DHC	District Heating and Cooling
HVAC	Heating, Cooling, Ventilation, and Air Conditioning
IEA	International Energy Agency
ISC	Interstate Council for Standardization, Metrology and Certification
ISC	Interstate Council for Standardization, Metrology and Certification
ISO	International Standard Organization
ISO	International Standard Organization
PD	Percentage of Dissatisfaction
PD	Percentage of Dissatisfaction
PMV	Predicted Mean Vote
PMV	Predicted Mean Vote
PPD	Predicted Percentage Dissatisfied
PPD	Predicted Percentage Dissatisfied
RHC	Radiant Heating and Cooling
RMS	Root Mean Square
RMS	Root Mean Square
RTE	Radiative Transfer Equation
RTE	Radiative Transfer Equation
SST	Shear Stress Transport
SST	Shear Stress Transport
M	Metabolic rate

P	Static pressure
T	Temperature
W	Effective mechanical power
e	Internal energy
k	Thermal conductivity
t	Time
u	Velocity vector component x
v	Velocity vector component y
w	Velocity vector component z
ρ	Density
τ	Viscous stresses

List of Tables

List of Figures

Chapter 1 – Introduction

1.1. Background

Nowadays, more than 90% of the population spend their lives indoors. The quality of the thermal comfort environment that surrounds us must be well adapted to the body temperature since we tend to spend most of our time indoors [1]. Therefore, today's energy consumption has increased to meet people's needs for electricity, hot water, and heating or cooling of rooms.

As a result of high energy consumption, burning fuels leads to global warming. Global warming is widely known as one of the major problems caused by human activities, so dealing with it is a significant challenge today. It is necessary to limit the demand for fossil fuels to keep the climate stable.

The distribution of energy consumption (Figure 1.1, a) shows that the industrial sector ranks first, followed by the transport sector in second place, and the household sector in third place, based on the International Energy Agency (IEA) [2]. According to the breakdown of total energy consumption by the IEA [2], a significant percentage corresponds to the residential sector, which accounts for 21.24% and attracts the interest of engineers. In addition, the IEA found that almost half (48.03%) of energy consumption is used for space heating within the residential sector [3].

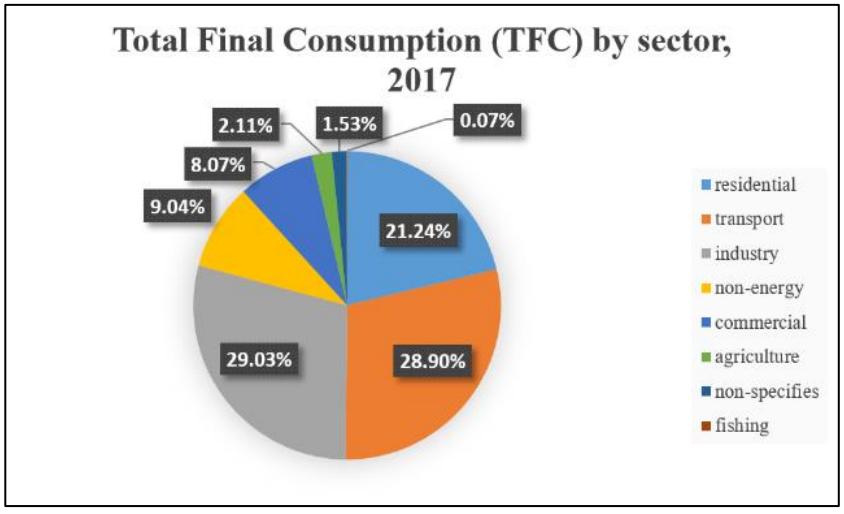

(a)

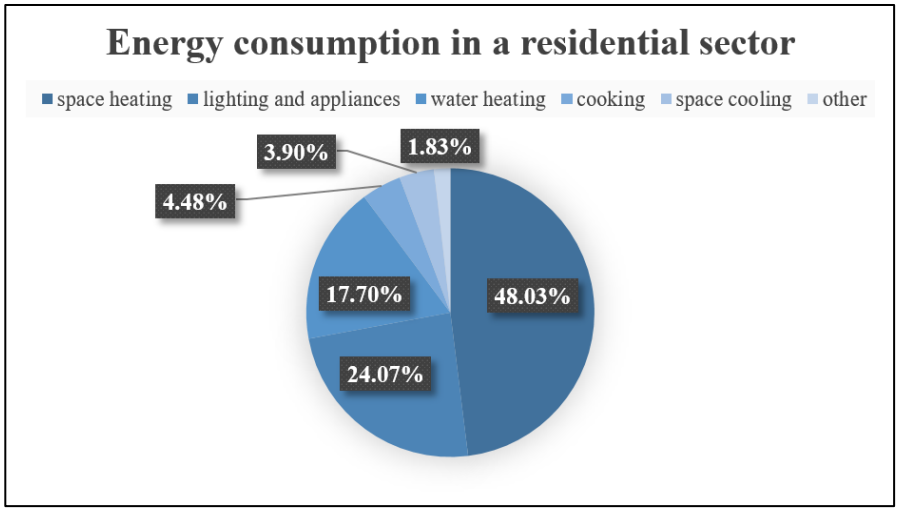

(b)

Figure 1.1: The breakdown of energy consumption: a) general sector; b) residential sector [2]

Reducing energy consumption leads to various outcomes such as financial savings in terms of cost, environmental friendliness, and high thermal efficiency. Therefore, energy-efficient heating systems are nowadays widely used for residential heating.

1.2. Motivation

The above statistics on total energy consumption are considered to study the reduction of residential energy consumption and thermal comfort. Researchers have extensively carried out the study of energy consumption and improvement of indoor thermal comfort using different types of heating systems under different conditions. However, most of the research has been carried out to improve the heating of the whole room as it is a traditional way of heating. The core idea of this research is to develop a concept for smart heating systems that heat only the people who are in the room.

1.3. Research Objectives

The main objective of this investigation is to assess the ability to directly heat an occupant in an enclosed space with an energy-efficient heating system, rather than heating the entire space, to reduce energy consumption while maintaining an acceptable level of thermal comfort at the human body surface. Focused heating might make more economic sense under the given conditions to provide comfortable heating to indoor occupants.

Chapter 2 – Literature Review

2.1. Overview on space heating systems

Residential heating, cooling, ventilation, and air conditioning (HVAC) systems are designed so that their functionality provides energy savings and heat conservation, as well as a comfortable living environment. Therefore, the goal of HVAC design engineers is to determine the optimal space heating system with the appropriate equipment, taking into account both economic and environmental factors.

Following the guidelines and analysis in ASHRAE [4], a choice is made between centralized and decentralized primary heating and cooling systems, and then one of the options is selected for heating and cooling distribution to the end-user (Figure 2.1).

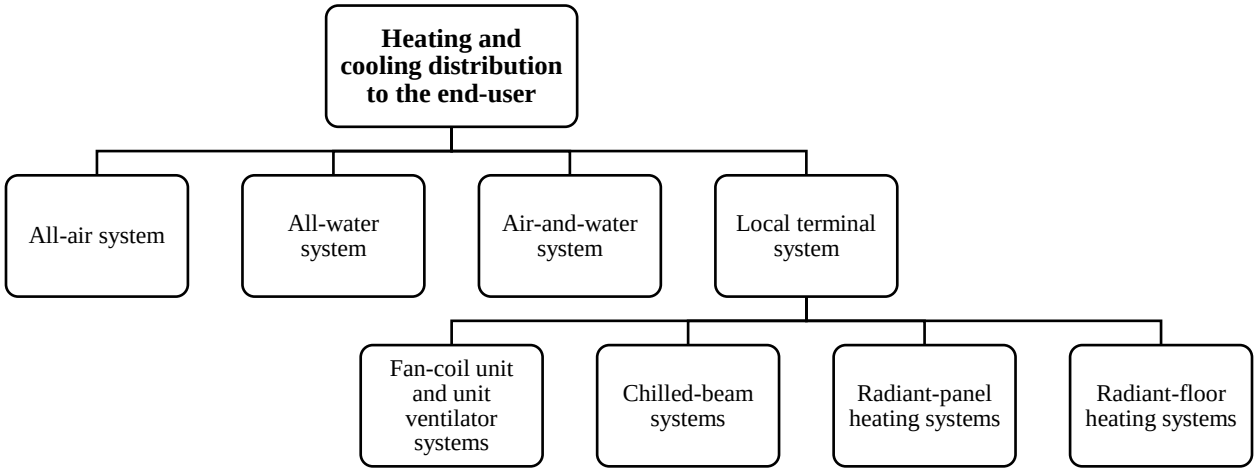

Figure 2.1: Distribution of heating and cooling systems to consumers [4]

Most residential buildings use district heating and cooling (DHC) systems, primarily operated by panel radiant heating and cooling systems. District heating and cooling supply thermal energy from a central plant through the distribution network to residential, commercial, and industrial customers who use it for heating, cooling, and water heating. The central plant, the distribution network, and the consumer systems are thus the three main components of this system (Figure 2.2) [4, 5].

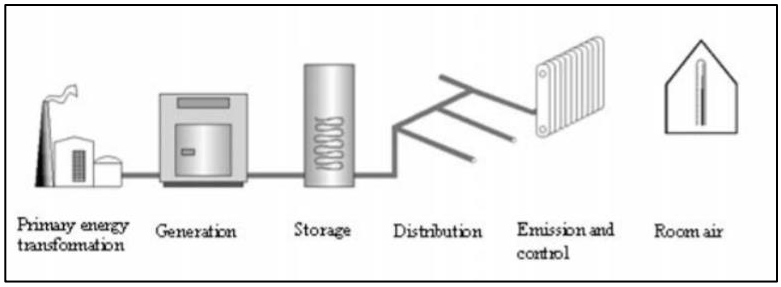

Figure 2.2: Schematic diagram of district heating system [6]

In the literature, radiant heating and cooling (RHC) systems tend to be used to refer to a radiant heat transfer that accounts for more than 50% of heat exchange inside a conditioned environment. More importantly, radiation exchange between the radiant surfaces and the inhabitants achieves a preferable thermal comfort environment due to the lower air temperature difference in the radiant heating buildings [7].

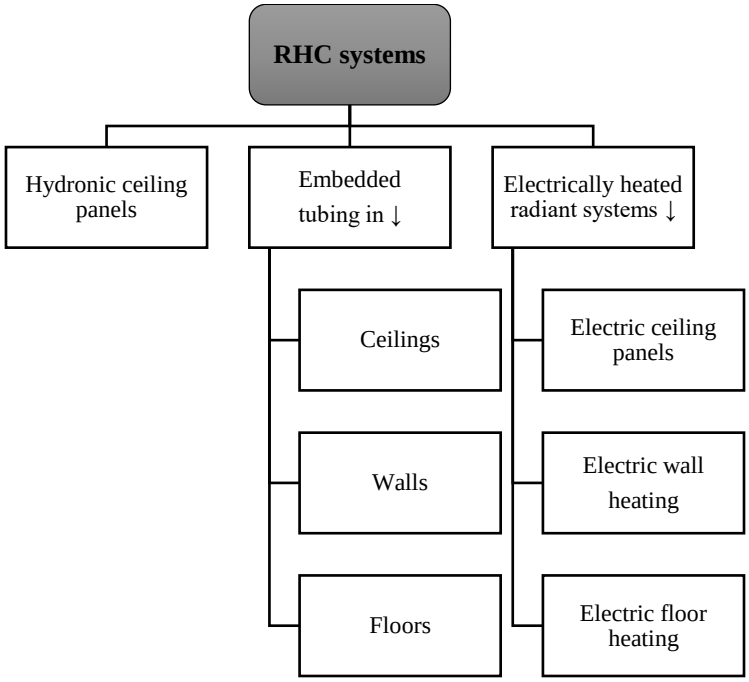

Figure 2.3: The most common used RHC systems [4]

Panel radiators, also known as conventional radiators, are commonly studied types of heating devices and systems in residential buildings in European and Asian countries [8]. Several studies, for instance [9-12], have been conducted on water-filled panel radiators compared to other heating systems.

In [9], the authors examined a study of a conventional heating system, namely a low water temperature heating panel, using CFD simulations. The result was that the warm air from the radiator mixed well with the cold air to maintain the comfort and healthy environment in the occupied zone at an acceptable level, based on the guidelines in ISO 7730:1994. Therefore, using a low water temperature radiator in residential buildings is preferable to other heating systems because it generates energy more efficiently, reduces heat loss, and the indoor air quality is more uniform and stable at low-temperature differences. Similarly, Sarbu and Sebarchievice [10] concluded that low water inlet and outlet temperature panel radiators perform well in indoor thermal comfort, efficient energy consumption, and environmental friendliness. As noted by Hasan et al. [11], CFD simulations of a heated room with radiators showed that an occupied zone remained in the comfort zone when the air temperature of the area room was above 20°C. It was also suggested that combining a low water temperature heating system and a decentralized heating system (heat pumps) would efficiently produce heat. In their literature review, Ovchinnikov and et al. [12] examined a comparative review of recent research and advances in space heating systems for low-temperature water heating to evaluate their performance in cold climates. The result was that low-temperature heating provides higher or the same comfort to the occupants compared to the other heating systems. Therefore, it was recommended that low-temperature water heating systems could be used in cold weather. It was also found that condensing boilers, heat pumps, and waste heat are the most efficient sources of space heating.

2.2. Experimental study

The first studies on space heating systems were experimentally investigated by Olsen [13], and other researchers also used it as a comparative study and referred to his work. The test room was heated with nine different heating systems, including a well-insulated room and a double-glazed window under winter conditions. The result was a comfortable environment in the room with all heating systems. However, it is recommended to place the radiator on the wall exposed to the outdoor environment to maintain the comfort zone near the window.

In the last decade, using a numerical simulation tool has gained importance due to the development and advancement in computer technology and the accessibility of commercial software [14]. Computational Fluid Dynamics (CFD) is a well-known tool for evaluating HVAC systems for various indoor environments such as buildings and vehicles, which provides the

temperature profiles and velocity fields [15]. It has been experimentally studied and proved that the CFD approach is practical, less time-consuming, and cost-effective [16]. Therefore, the CFD approach is a common practice for performing simulations of the HVAC system in buildings [17].

2.3. Numerical study

A growing number of CFD numerical studies have been conducted on space heating systems that use various types of heating equipment to reduce energy consumption while providing thermal comfort to occupants. The numerical work by Raczkowski et al. [18] presented the results of a CFD simulation of the natural ventilation performance in a room during the heating season. Similarly, Risberg et al. [19] studied a low-energy building rather than individual rooms to create computer setups for indoor climate simulations CFD. The capability and accuracy of CFD simulation of a heated room were studied by Teodosiu [20] to compare with experimental data. The result was quite accurate with the experimental data provided. Several other numerical studies [21-23] investigated a CFD simulation model of a $3D$ room with a radiator heating system to analyze the thermal comfort under different room conditions.

Table 2.1: Major findings on space heating in research studies [24-34]

#	Research work	Geometry of 3D room model (inlet and outlet locations)	Methods	Objective	Main findings
1	Myhren, J. A., & Holmberg, S. (2008) [24]	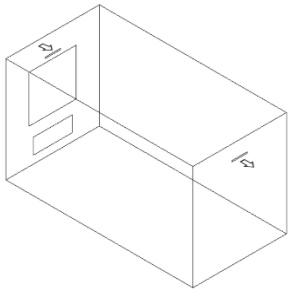	Numerical study, CFD	The comparative numerical analysis between low and high temperature heating systems on thermal comfort within the space	• The occupied zone was maintained at a steady 22℃ as the cold air from the supply vent came into contact with the radiator, resulting in thorough mixing of the warm air around the occupant • In the case of underfloor and wall heating systems, a seated occupant may be annoyed by a cold air flow of $0.15\ m/s$. Therefore, the average air velocity in the occupied area should be less than the specified $0.15\ m/s$.

2	Bohojło, A. (2011) [25]	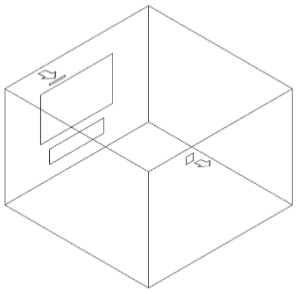	Numerical study, CFD	Investigation of thermal comfort in a living room with a certain type of ventilation and radiator heating	• The trickle ventilation system showed the discomfort of the occupants: 40.3% felt dissatisfied and cold
3	Sevilgen, G., & Kilic, M. (2011) [26]	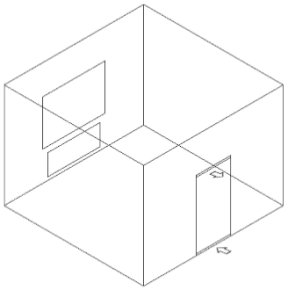	Numerical study, CFD	Using a virtual mannequin, the researchers investigated the relationship between heating power and thermal comfort of two-panel radiators. They obtained the airflow, temperature and thermal properties by experimenting with different heat transfer values and radiator surface temperatures	• Installing a panel radiator with a high surface temperature usually reduces the discomfort caused by cold windows; however, better insulating wall and window components can remedy the situation even more effectively
4	Horikiri, K. et al. (2014) [27]	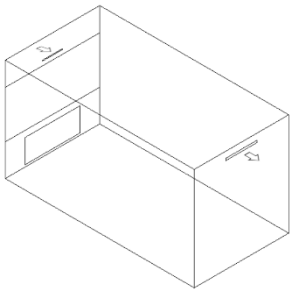	Experimental and numerical study, CFD	In terms of comfort criteria, a 3-D forced ventilation system with a heat source and different wall thicknesses and window glass were investigated	• In a forced ventilation system, cold winter temperatures require a large-surface radiator, well-insulated walls, and low thermal conductivity of the walls

5	Errebai, F. B. et al. (2017) [28]	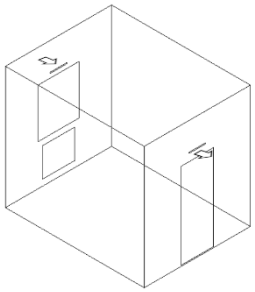	Numerical study, CFD	Evaluation of thermal comfort in a living space using air temperature profiles of different heating systems	• Underfloor heating is the best choice if the positions of the supply and exhaust vents are opposite each other and maintain a comfortable occupied zone
6	Raczkowski, A. et al. (2018) [29]	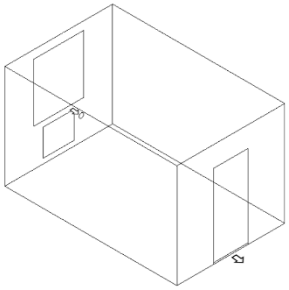	Numerical study, CFD	Using CFD simulations in a naturally ventilated room, create and test a three-dimensional heat transfer model with improved inlet placement	• Placing the supply air valve $2.2\ m$ above the floor provides good mixing of the cold and hot air, so that the required thermal comfort is achieved sooner than placing the supply air valve below the window
7	Rabanillo-Herrero, M. et al. (2019) [30]	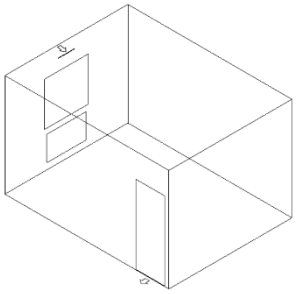	Experimental and numerical study, CFD	In winter, evaluate the air temperature and thermal comfort of three different heating systems by changing their placement	• Placing the heater under the window or air intake (near the cold area) resulted in an acceptable comfort level in the room

8	Karacavus, B., & Aydin, K. (2019) [31]	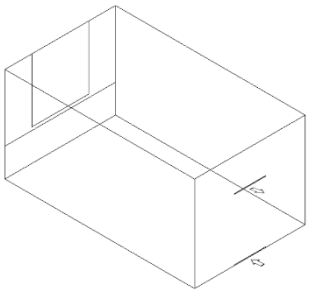	Numerical study, CFD	Numerical study of general and local thermal comfort with two different arrangements of the panel radiator under the window, the other on the ceiling, and three different outdoor temperatures according to the standard ISO 7730.	• At colder outdoor temperatures, good insulation of the walls is required and the surface area of the panel radiator must be increased
9	Khalil, E. E., & Sobhi, M. (2020) [32]	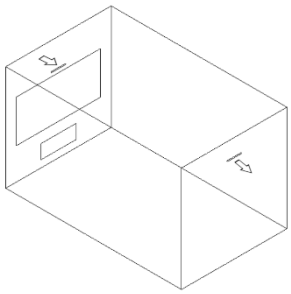	Numerical study, CFD	A CFD -based coupled natural convection and radiation analysis approach was used to study the thermal environment in a living room	• The PMV and PPD - comfort parameters did not meet the recommended values for all given cases of heating systems with the given boundary conditions
10	Maher, D. et al. (2020) [33]	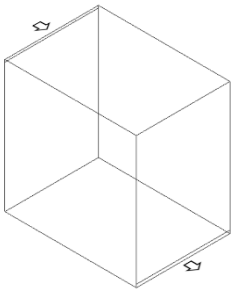	Numerical study, CFD	A comprehensive numerical study of airflow in an empty naturally ventilated 3D room was validated to give good agreement with experimental data	• The main result of this study was that the most significant value of air velocity was $0.15\ m/s$ and air temperature was 19℃ according to ADPI criteria

11	Anthony, A. S., & Verma, T. N. (2021) [34]	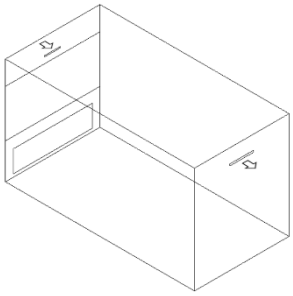	Numerical study, CFD	The difference in thermal comfort between the head and foot areas in a room heated by a radiator was evaluated using two methods: Operative Temperature and Comfort Temperature	• Numerically derived results of the operative and comfort temperatures gave a comfortable environment that is between 20℃ and 22℃ in the winter season

In [24-34], the authors point out that using radiant heating systems for space heating in residential buildings provides better comfort than air-only systems. The essential features of these systems include less air movement and uniform temperature gradient, and comfortable indoor air quality in the room. However, our proposed method of space heating used the smallest commercially available size of radiant heater commercially available to compare with the standard sizes of radiant panels used in the above literature. Therefore, this investigation focused on the overhead radiant heaters with small dimensions and not on the side radiant heaters placed on the wall exposed to the outside temperature.

2.4. Computational Thermal Manikin

Computational Thermal Manikin (CTM) has been identified as an actual human body model to analyze heat loss and evaluate thermal comfort in CFD modeling under different indoor conditions. There are different types of CTM based on the geometry and shapes, which can be simplified with rectangular, cylindrical, and complicated like a scanned human. CTMs with simple geometries usually have a lower computational cost because they can use a larger computational grid size. On the other hand, simple geometries can cause local airflow details to be lost at CTM surfaces, although the impact on airflow in bulk regions is small [35].

Miyanaga et al. [36] conducted a comprehensive study on a simplified CTM by designing the model with rectangles and cylinders to investigate the validation of the geometry with experimental data. It was shown that the simplified body geometry should be based on the body

shape of a real person and that the simulation of the simplification must be performed correctly. Therefore, the results were very similar to those of the original body shape, and the geometric correctness of the model was confirmed (Figure 2.4).

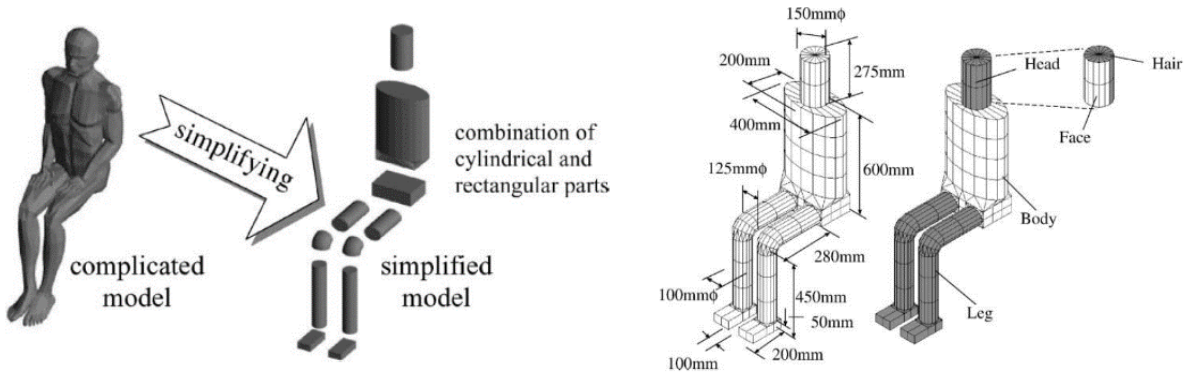

(a) (b)

Figure 2.4: The simplification of actual human dimensions into CTM [36]

Cropper et al. [37] conducted a numerical study of thermal comfort around the virtual mannequin in a standing position using the CFD model, as it accurately predicts airflow temperature and velocity near the occupant. The computational thermal manikin was constructed with 19 body elements and clothing on the human. The geometry of the manikin was optimized to obtain a fine CFD mesh, especially around the arms and hands. In [38], the authors analyzed a breathing thermal manikin to evaluate human heat loss in terms of thermal comfort within a personalized ventilation system. For this work, the CTM was constructed with mouth and nose segments to represent 16 parts of the body. It is strongly recommended to validate the CTM simulation results with experimental data under the same conditions.

There are a considerable number of comparative tests on heat loss, which have been studied by Nielsen et al. [39], [40], and Nielsen et al. [41]. Nielsen et al. [39, 40] presented a benchmark test of the manikin in a CFD modeling to develop it for further simple and straightforward use. This provides experimental data that can be used as a comparative study for future use. Furthermore, in another paper [41], the authors have shown that CFD modeling of heat loss from manikins can be combined with new benchmark heat loss tests and standardized assessment techniques for comfort assessment.

2.5. Thermal Comfort

Nowadays, engineers try to achieve a high level of comfort in the design of rooms, buildings, and enclosed spaces. Therefore, local and international standards guide and develop engineers in designing a high-quality indoor environment. Markov [1] conducted a review study to specify the primary international thermal comfort standards that are commonly used in the world. Due to the availability and reliability of the sources, we have used two international standards in this study that are closely related to thermal comfort and the environment (Figure 2.5).

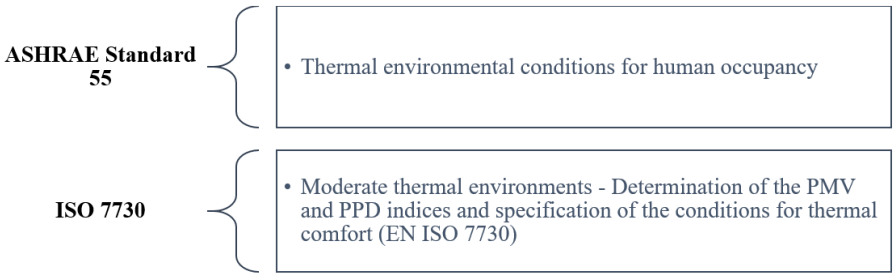

Figure 2.5: The most widely used international standards [1]

2.5.1. ISO 7730 International Standard

ISO 7730 International Standard consists of methods for predicting indoor and local thermal comfort. The standard presents an analytical method for calculating two variables for thermal comfort, namely PMV (Predicted Mean Vote) and PPD (Predicted Percentage of Dissatisfied). Local thermal discomfort is assessed in addition to PMV and PPD to define the range of acceptable human comfort [42].

1.5.2. ASHRAE Standard 55-2017

ANSI /ASHRAE Standard 55-2017 is a set of written rules to provide occupants with an acceptable thermal environment in space. This standard aims to determine the combination of thermal environmental factors and personal factors in indoor spaces that create an acceptable comfort environment for occupants in an enclosed space. The PMV and PPD indices should be

applied when using analytical methods to determine the acceptable thermal environment for the occupants of an enclosed space [43].

2.5.3. Predicted mean vote (PMV)

The PMV is an indicator for predicting the mean of the votes of many people on a seven-point scale for thermal sensation (Table 2.2), corresponding to the thermal balance of the human body.

Table 2.2: A 7-point scale of thermal sensation

Cold	**Cool**	**Slightly cool**	**Neutral**	**Slightly warm**	**Warm**	**Hot**
-3	**-2**	**-1**	**0**	**+1**	**+2**	**+3**

The calculating formula for PMV value as written in [42, 43]:

$$PMV = [0{,}303e^{-0.036M} + 0{,}028] \times \begin{bmatrix} (M-W) - 3{,}05\times10^{-3}[5\,733 - 6{,}99(M-W) - p_a] - 0{,}42[(M-W) - 58{,}15] \\ -1{,}7\times10^{-5}M(5\,867 - p_a) - 0{,}0014M(34 - t_a) \\ -3{,}96\times10^{-8}f_{cl}[(t_{cl}+273)^4 - (\bar{t}_r+273)^4] - f_{cl}h_c(t_{cl}-t_a) \end{bmatrix} \quad (2.1)$$

$$t_{cl} = 35{,}7 - 0{,}028(M-W) - I_{cl}\{3{,}96\times10^{-8}f_{cl}[(t_{cl}+273)^4 - (\bar{t}_r+273)^4] + f_{cl}h_c(t_{cl}-t_a)\} \quad (2.2)$$

$$h_c = \begin{cases} 2{,}38|t_{cl}-t_a|^{0{,}25} & for \quad 2{,}38|t_{cl}-t_a|^{0{,}25} > 12{,}1\sqrt{v_{ar}} \\ 12{,}1\sqrt{v_{ar}} & for \quad 2{,}38|t_{cl}-t_a|^{0{,}25} < 12{,}1\sqrt{v_{ar}} \end{cases} \quad (2.3)$$

$$f_{cl} = \begin{cases} 1{,}00 + 1{,}290l_{cl} & for \quad l_{cl} \le 0{,}078 m^2K/W \\ 1{,}05 + 0{,}645l_{cl} & for \quad l_{cl} > 0{,}078 m^2K/W \end{cases} \quad (2.4)$$

where M is metabolic rate (W/m^2); W is effective mechanical power (W/m^2); I_{cl} is clothing insulation (m^2K/W); f_{cl} is clothing surface area factor; t_a is air temperature (℃); $\bar{t}_r$ is mean radiant temperature (℃); v_{ar} is relative air velocity (m/s); p_a is water vapour partial pressure (Pa); h_c is convective heat transfer coefficient [$\frac{W}{m^2\cdot K}$]; t_{cl} is clothing surface temperature (℃).

2.5.4. Predicted Percentage Dissatisfied (PPD)

The PPD is an indicator that forms a meaningful prediction of the percentage of thermally dissatisfied people who feel too cool and too warm [42, 43]. The above table is given to participants in a room to match their thermal sensation to the indoor environment.

The following formula was used to calculate the PPD value after determining the PMV equations in (2.1):

$$PPD = 100 - 95e^{(-0{,}033\,53PMV^4 - 0{,}217\,9PMV^2)} \tag{2.5}$$

2.5.5. Vertical air temperature difference

This factor is caused by the temperature difference between the head and the ankles of the human body, which results in a vertical air temperature difference. Figure 2.6 shows a curve describing the percentage of dissatisfaction (PD), which is a function of the vertical air temperature difference between the head and ankles [42]. Also, the following formula is used to calculate PD:

$$PD = \frac{100}{1 + \exp(5{,}76 - 0{,}856\Delta t_{a,v})} \tag{2.6}$$

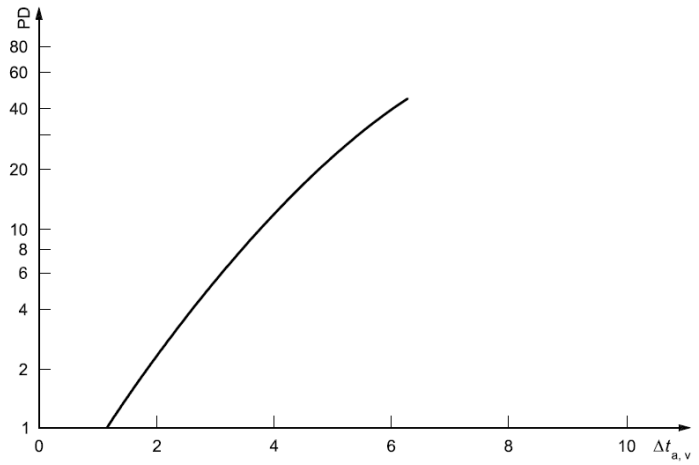

Figure 2.6: PD as function of vertical air temperature difference [42]

Chapter 3 – Methodology

3.1. Overview

This chapter begins by establishing the methodology followed from the beginning to the end of the thesis. Figure 3.1 shows the simulation methodology used in the current numerical study for the model CFD. First, the simplified geometry of the CTM and the domain of CFD must be determined; then, the correct boundary conditions are established considering the same experimental conditions. After that, it is essential to verify and validate the performance of the model CFD following experimental data to accurately represent the indoor operating environment [14, 16]. In this study, the model CFD, after meeting the validation criteria, is defined as a reference case for the implementation of heating systems that aim to achieve thermal comfort and calculate energy consumption.

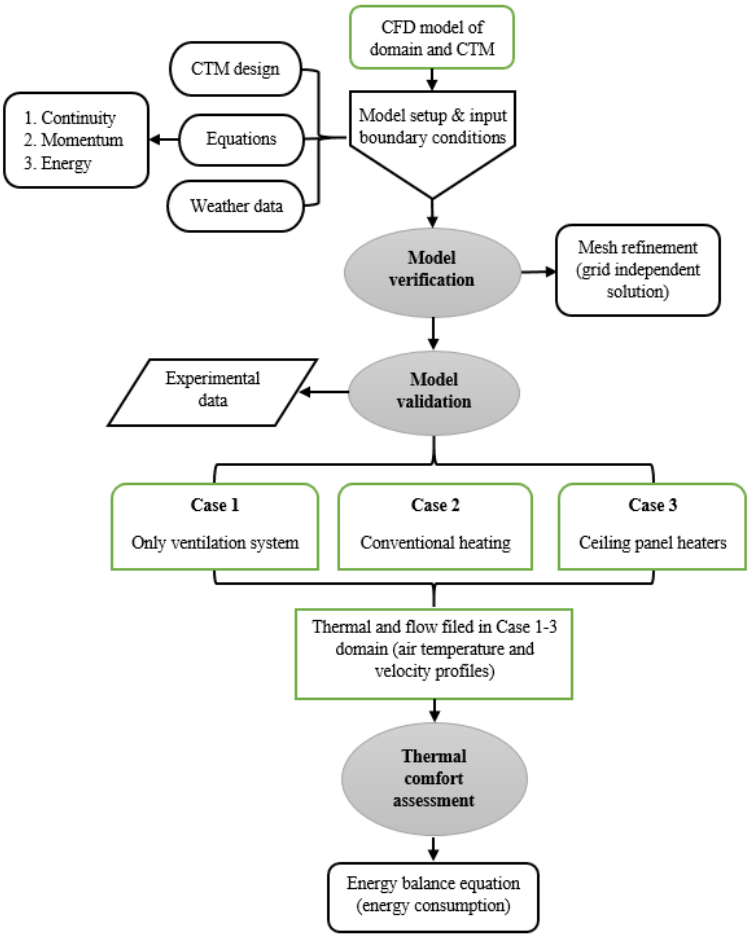

Figure 3.1: Methodology of the present CFD numerical analysis [14, 16]

3.2. Design of CTM

The simulation model of the occupant in the indoor environment was adopted from the research study by Sørensen and Voigt [44]. The numerical study used a ready-to-use manikin with a seated human body in an enclosed space. However, the research dates back to 2003, and the available link for the manikin did not work to use it.

A new simplified geometry of the human manikin is constructed using the ANSYS DesignModeler software within the enclosed space. As mentioned earlier and noted by Miyanaga et al. [36], CTM modeling considered the average dimensions of the person and constructed mainly cylindrical and elliptical shapes based on the complex shape (Figure 3.2). Thus, the surface area of a whole-body deviates by $0.16\ m^2$ because detailed body parts such as the face, hands, and chest were simplified (Figure 3.2).

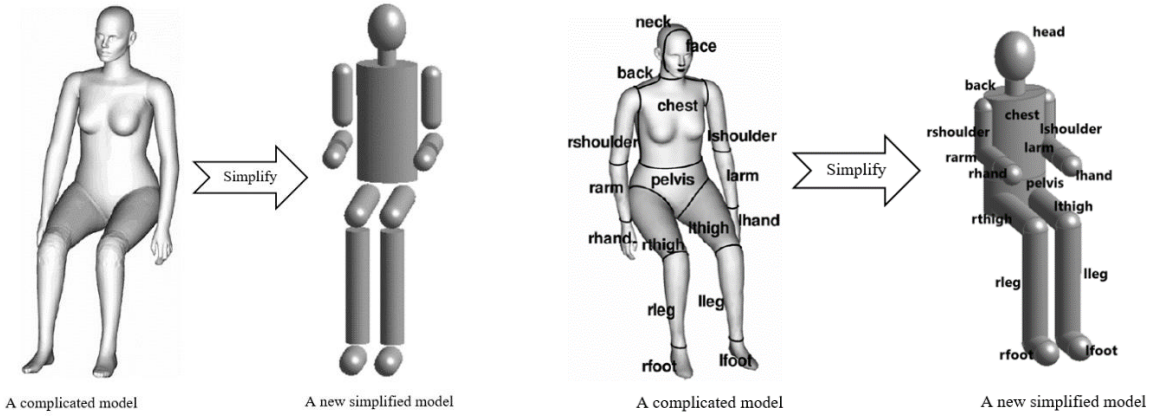

(a) (b)

Figure 3.2: A geometry of CTM: a) simplified model; b) body parts [44]

3.3. Geometry of the CFD domain

The heat transfer and natural convection flow around CTM are investigated numerically in a 3D space with dimensions $L(x) \times H(y) \times W(z) = 2.95\ m \times 2.95\ m \times 2.4\ m$ (Figure 3.3) agrees with the experimental data in [44]. At the height of $z = 1.34\ m$, the manikin was positioned so that the tip of the nose was midway between the walls $(x = y = 1.475\ m)$. The feet were 0.02 m above the floor at this position.

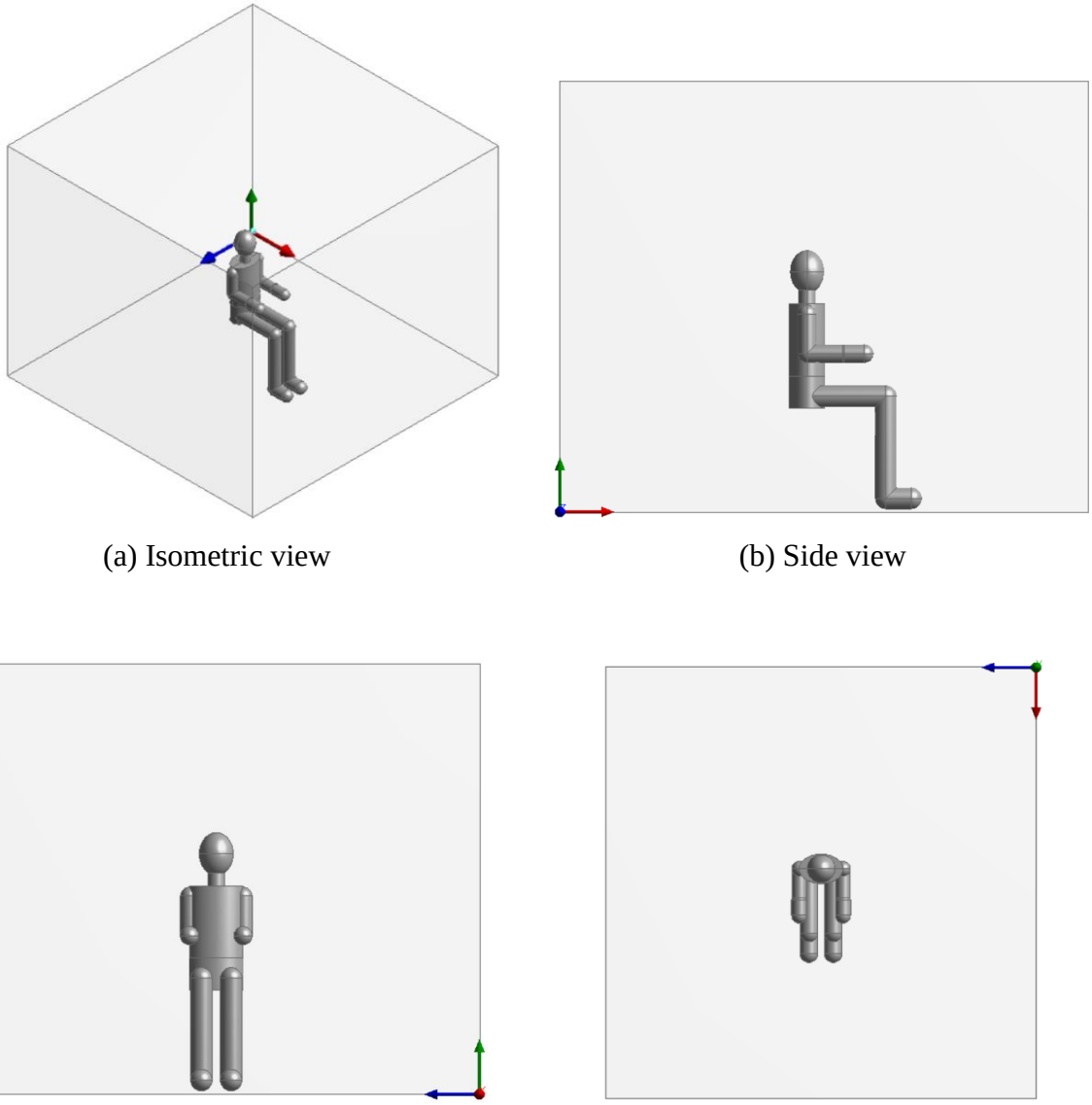

(a) Isometric view (b) Side view

(c) Front view (d) Top view

Figure 3.3: A redesigned CTM in a seated position in an enclosed space with a modified and simplified geometry scheme

3.4. Governing Equations

The analysis of a three-dimensional airflow and the heat transfer of the numerical model was solved using the software ANSYS CFX [45]. The basic equations of fluid dynamics - the continuity, momentum, and energy equations - were solved for the incompressible and continuous

flow. The following formulas for the continuity, momentum, and energy equations were written in the conservation form according to Wendt [46] and Lopez-Ruiz [47]:

- *The continuity equation*

$$\frac{\partial \rho}{\partial t} + \nabla \times \left(\rho \vec{V}\right) = 0 \tag{3.1}$$

- *The momentum equation*

x-direction component ($\hat{\imath}$)

$$\frac{\partial (\rho u)}{\partial t} + \nabla \times \left(\rho u \vec{V}\right) = -\frac{\partial P}{\partial x} + \frac{\partial \tau_{xx}}{\partial x} + \frac{\partial \tau_{yx}}{\partial y} + \frac{\partial \tau_{zx}}{\partial z} + \rho f_x \tag{3.2}$$

y-direction component ($\hat{\jmath}$)

$$\frac{\partial (\rho v)}{\partial t} + \nabla \times \left(\rho v \vec{V}\right) = -\frac{\partial P}{\partial y} + \frac{\partial \tau_{xy}}{\partial x} + \frac{\partial \tau_{yy}}{\partial y} + \frac{\partial \tau_{zy}}{\partial z} + \rho f_y \tag{3.3}$$

z-direction component ($\hat{k}$)

$$\frac{\partial (\rho w)}{\partial t} + \nabla \times \left(\rho w \vec{V}\right) = -\frac{\partial P}{\partial z} + \frac{\partial \tau_{xz}}{\partial x} + \frac{\partial \tau_{yz}}{\partial y} + \frac{\partial \tau_{zz}}{\partial z} + \rho f_z \tag{3.4}$$

- *The energy equation*

$$\begin{aligned} &\frac{\partial}{\partial t}\left[\rho\left(e + \frac{u^2 + v^2 + w^2}{2}\right)\right] + \nabla \times \left[\rho\left(e + \frac{u^2 + v^2 + w^2}{2}\right)\vec{V}\right] \\ &\quad = \rho \dot{q} + \frac{\partial}{\partial x}\left(k\frac{\partial T}{\partial x}\right) + \frac{\partial}{\partial y}\left(k\frac{\partial T}{\partial y}\right) + \frac{\partial}{\partial z}\left(k\frac{\partial T}{\partial z}\right) - \frac{\partial (uP)}{\partial x} - \frac{\partial (vP)}{\partial y} \\ &\quad - \frac{\partial (wP)}{\partial z} + \frac{\partial (u\tau_{xx})}{\partial x} + \frac{\partial (u\tau_{yx})}{\partial y} + \frac{\partial (u\tau_{zx})}{\partial z} + \frac{\partial \left(v\tau_{xy}\right)}{\partial x} + \frac{\partial \left(v\tau_{yy}\right)}{\partial y} \\ &\quad + \frac{\partial \left(v\tau_{zy}\right)}{\partial z} + \frac{\partial (w\tau_{xz})}{\partial x} + \frac{\partial (w\tau_{yz})}{\partial y} + \frac{\partial (w\tau_{zz})}{\partial z} + \rho \vec{f} \times \vec{V} \end{aligned} \tag{3.5}$$

where u, v and w are velocity vector components; e is an internal energy; $\vec{f}$ is body forces; k is thermal conductivity; P is a static pressure; $\dot{q}$ is heat transfer; t is time; T is temperature; ρ is

density; τ is viscous stresses; and $\nabla = \frac{\partial}{\partial x}\vec{\imath} + \frac{\partial}{\partial y}\vec{\jmath} + \frac{\partial}{\partial z}\vec{k}$ is the gradient vector operator for Cartesian coordinates.

Many numerical studies have shown that the above equations must be supplemented by suitable initial and boundary conditions.

3.5. Turbulence Model

Specifying the most appropriate turbulence model for CFD simulation is essential in numerical analysis. Three main turbulence models, such as Standard k-ε, Standard k-ω, and Shear Stress Transport (SST), were implemented to achieve an accurate validation with the agreement to experimental data [48, 49].

- *The Standard k-ε model*

The k-ε model often referred to as the standard k-ε model, can provide reasonably accurate results for flows with free shear layers and low-pressure gradients [48]. The Standard k-ε model equation is defined below:

$$\frac{\partial(\rho k)}{\partial t} + \text{div}(\rho k U) = div\left[\frac{\mu_t}{\sigma_k}\text{grad}\, k\right] + 2\mu_t S_{ij} \cdot S_{ij} - \rho\varepsilon \tag{3.6}$$

$$\underbrace{\frac{\partial(\rho\varepsilon)}{\partial t}}_{\text{Rate of change of } k \text{ or } \varepsilon} + \underbrace{\text{div}(\rho\varepsilon U)}_{\text{Transport of } k \text{ or } \varepsilon \text{ by convection}} = \underbrace{div\left[\frac{\mu_t}{\sigma_\varepsilon}\text{grad}\,\varepsilon\right]}_{\text{Transport of } k \text{ or } \varepsilon \text{ by diffusion}} + \underbrace{C_{1\varepsilon}\frac{\varepsilon}{k}2\mu_t S_{ij} \cdot S_{ij}}_{\text{Rate of production of } k \text{ or } \varepsilon} - \underbrace{C_{2\varepsilon}\rho\frac{\varepsilon^2}{k}}_{\text{Rate of destruction of } k \text{ or } \varepsilon} \tag{3.7}$$

$C_\mu = 0.09$ $\sigma_k = 1.00$ $\sigma_\varepsilon = 1.30$ $C_{1\varepsilon} = 1.44$ $C_{2\varepsilon} = 1.92$

- *The Standard k-ω model*

The k-ω turbulence model is an eddy viscosity model that is well known and widely used. It has been shown that the k-ω model is numerically more stable than the k-ε model, especially in the viscous sublayer near the wall [48]. The following equations of the Standard k-ω model are given:

$$\frac{\partial(\rho k)}{\partial t} + \text{div}(\rho k U) = div\left[\left(\mu + \frac{\mu_t}{\sigma_k}\right)\text{grad}\, k\right] + P_k - \beta^* \rho k \omega \tag{3.8}$$

$$P_k = \left(2\mu_t S_{ij} \cdot S_{ij} - \frac{2}{3}\rho k \frac{\partial U_i}{\partial x_j}\delta_{ij}\right) \tag{3.9}$$

$$\underbrace{\frac{\partial(\rho\omega)}{\partial t}}_{\substack{\text{Rate of change of } k \text{ or } \omega}} + \underbrace{\text{div}(\rho\omega U)}_{\substack{\text{Transport of } k \text{ or } \omega \text{ by convection}}} =$$

$$= \underbrace{div\left[\left(\mu + \frac{\mu_t}{\sigma_\omega}\right)\text{grad}\, \omega\right]}_{\substack{\text{Transport of } k \text{ or } \omega \text{ by diffusion}}} + \underbrace{\gamma_1\left(2\rho S_{ij} \cdot S_{ij} - \frac{2}{3}\rho\omega \frac{\partial U_i}{\partial x_j}\delta_{ij}\right)}_{\substack{\text{Rate of production of } k \text{ or } \omega}} - \underbrace{\beta_1 \rho \omega^2}_{\substack{\text{Rate of destruction of } k \text{ or } \omega}} \tag{3.10}$$

$$+\gamma_1\left(2\rho S_{ij} \cdot S_{ij} - \frac{2}{3}\rho\omega \frac{\partial U_i}{\partial x_j}\delta_{ij}\right) - \beta_1 \rho \omega^2 \tag{3.11}$$

$\sigma_k = 2.0$ $\sigma_\omega = 2.0$ $\gamma_1 = 0.553$ $\beta_1 = 0.075$ $\beta^* = 0.09$

- *The Shear Stress Transport (SST) model*

On solid walls, this model uses the Standard k-ω model, while near boundary layer edges and in layers with free shear, it uses the Standard k-ε model. SST modeling combined with vortex modification improves the prediction of flows with large pressure gradients and detachments [48]. The equation for the SST model is as follows:

$$\frac{\partial(\rho k)}{\partial t} + \text{div}(\rho k U) = div\left[\left(\mu + \frac{\mu_t}{\sigma_k}\right)\text{grad}\, k\right] + P_k - \beta^* \rho k \omega \tag{3.12}$$

$$\frac{\partial(\rho\omega)}{\partial t} + \mathrm{div}(\rho\omega U) = div\left[\left(\mu + \frac{\mu_t}{\sigma_{\omega,1}}\right)\mathrm{grad}\ \omega\right] + \gamma_2\left(2\rho S_{ij}\cdot S_{ij} - \frac{2}{3}\rho\omega\frac{\partial U_i}{\partial x_j}\delta_{ij}\right) - \beta_2\rho\omega^2 + 2\frac{\rho}{\sigma_{\omega,2}\omega}\frac{\partial k}{\partial x_k}\frac{\partial \omega}{\partial x_k} \quad (3.13)$$

$\sigma_k = 1.0$ $\sigma_{\omega,1} = 2.0$ $\sigma_{\omega,2} = 1.17$ $\gamma_2 = 0.44$ $\beta_2 = 0.083$ $\beta^* = 0.09$

where $C = F_C C_1 + (1 - F_C)C_2$ is cross-diffusion term, derived by blending transition functions between k-ε model and k-ω model.

3.6. Radiation Model

According to ANSYS-CFX Solver Guide [49], radiation modeling aims to solve the radiative transfer equation and derive the source term S for the energy equation and the radiative heat flux on walls. The radiative transfer equation (RTE) is given below:

$$\frac{dI_v(\boldsymbol{r},\boldsymbol{s})}{ds} = \left(-(K_{av}+K_{sv})I_v(\boldsymbol{r},\boldsymbol{s}) + K_{av}I_b(v,T) + \frac{K_{sv}}{4\pi}\int_{4\pi} dI_v(\boldsymbol{r},\boldsymbol{s}')\Phi(\boldsymbol{s}\cdot\boldsymbol{s}')d\Omega' + S\right) \quad (3.14)$$

where v is frequency; $\boldsymbol{r}$ is position vector; $\boldsymbol{s}$ directional vector; s is path length; K_a is the absorption coefficient; K_s is the scattering coefficient; I_b is the Blackbody emission intensity; I_v is the Spectral radiation intensity; T is local absolute temperature; Ω is solid angle; Φ is in-scattering phase function; S is the radiation intensity source term.

- *Diffusely emitting and reflecting opaque boundaries*

$$I_v(\boldsymbol{r}_\omega,\boldsymbol{s}) = \varepsilon_v(r_\omega)I_b(v,T) + \frac{\rho_\omega(\boldsymbol{r}_\omega)}{\pi}\int_{n\cdot s'<0} I_v(\boldsymbol{r}_\omega,\boldsymbol{s}')\,|\boldsymbol{n}\cdot\boldsymbol{s}'|d\Omega' \quad (3.15)$$

where ε_v is the spectral emissivity.

Rosseland, P1, Discrete Transfer, and Monte Carlo are four types of radiation models offered in ANSYS CFX [45]. According to ANSYS CFX [49], Monte Carlo or Discrete Transfer radiation models should be used for HVAC research. Therefore, Discrete Transfer and Monte

Carlo radiation models were used for the calculations, and the best model was subsequently selected for our CFD simulation. The surface-to-surface transfer model was chosen to calculate the radiant heat transfer using surface geometry view factors. In this model, heat is transferred by radiation between grey emitting surfaces in a closed environment.

3.7. Boundary Settings

In [44], the authors assumed that the entire ceiling was covered with cloth and the airflow was passing through it and that the floor was indicated as a supply air opening to create a vertical airflow (Figure 3.4). For the CTM, it was assumed that the body surface temperature was a constant 31℃. In addition, the walls were not insulated, so a constant temperature of 19.75℃ was assumed on all side walls, the floor, and the ceiling (Figure 3.4).

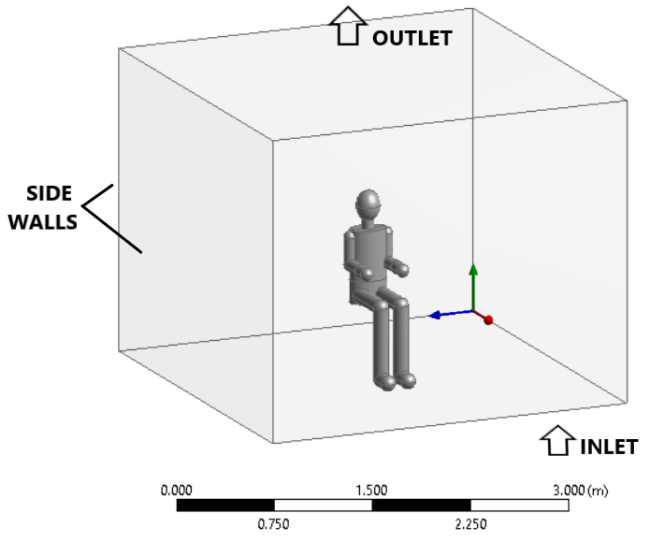

Boundary conditions [1]	
Inlet	$T_{air} = 19.75℃$ and $U_{air} = 0.02\ m/s$ Turbulence intensity - 30% Turbulence length - $0.004\ m$
Outlet	$T_{air} = 19.75℃$ and $0\ Pa$
Walls	$T_{wall} = 19.75℃$
CTM	$T_{CTM} = 31℃$ and $\varepsilon = 0.95$

Figure 3.4: Boundary Settings

Chapter 4 – Model Configuration

4.1. Mesh verification

The mesh was generated utilizing the commercial ANSYS CFX program, which offers a variety of grid refinement methods and great grid independence. The governing equations for each grid cell were solved and discretized using the Finite Volume Method [50]. The authors [51] state that the unstructured mesh facilitates the solution over a complex domain. Tetrahedral, pyramids, and prisms can be used for this purpose. The mesh in this study was created using tetrahedral elements (Figure 4.1).

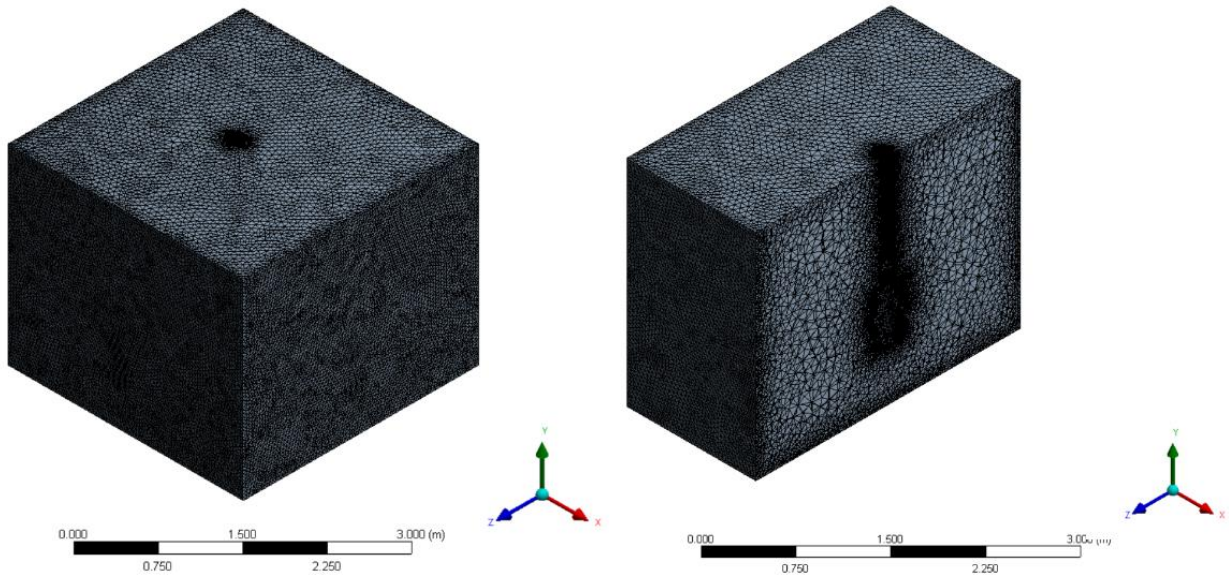

Figure 4.1: Mesh generation of CFD domain

To correctly represent the flow properties in the boundary regions, mesh inflation layers were formed around the occupant of the model [52]. The first layer thickness approach was used to construct five inflation layers with an initial layer height of $0.001\ m$ and a growth rate of 1.2 (Figure 4.2, a). The lowest orthogonal quality of the mesh was 0.153, and the maximum skewness was 0.85, which means that both mesh metrics were in an acceptable range (Figure 4.2, b, and c).

As we can see, the shape and structural quality of the average mesh were 'excellent and very good' according to the defined metric spectrum.

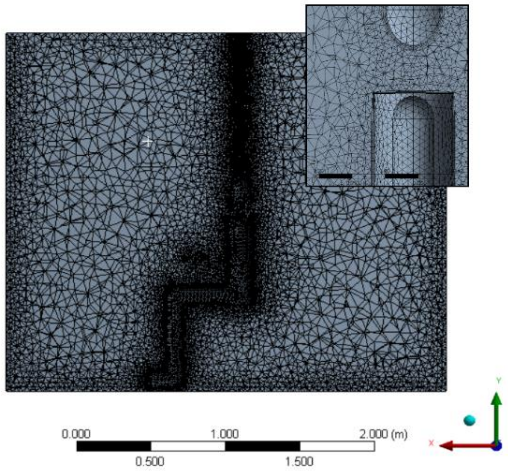

(a) Mesh inflation method

Mesh Metric	Skewness
Min	2.2616e-004
Max	0.84663
Average	0.22066
Standard Deviation	0.11823

(b) Skewness quality of final mesh

Mesh Metric	Orthogonal Quality
Min	0.15337
Max	0.99703
Average	0.77811
Standard Devi...	0.11687

(c) Orthogonal quality of final mesh

Figure 4.2: Refinement of the final mesh

A grid independence test was performed to evaluate the stability and performance of the numerical model by comparing the same scenario but with different mesh sizes [52]. This study performed mesh refinement simulations by refining the mesh by 50% of the previous mesh size (Figure 4.3, a). The air temperature profile at $z = 1.98$ m and the heat flux parameters were selected to compare the refined meshes (Figure 4.3, b). In addition, the temperature profile was divided into 10 points on the line running from the head of the CTM to the ceiling to calculate the root mean square error of temperature (RMS) (Table 4.1). Then, Mesh 3 with 324 3468 nodes was selected as the final mesh, as further refinements had no visible effect on the simulation results.

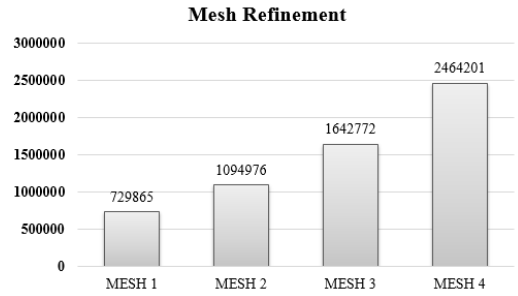

(a)

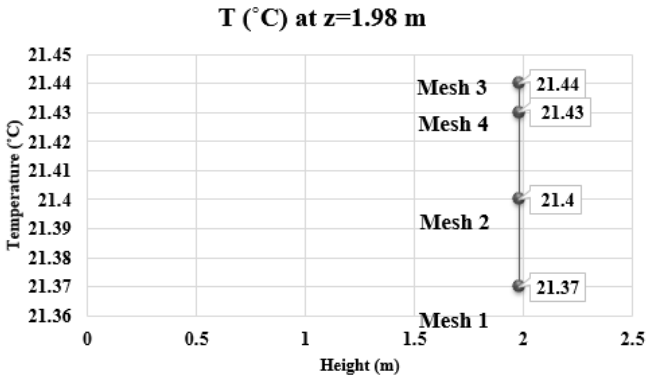

(b)

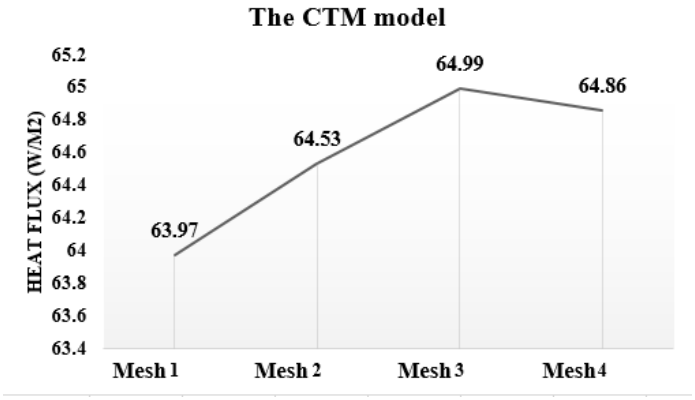

(c)

Figure 4.3: Mesh verification graphs

Table 4.1: Estimation of error between mesh refinements

	Mesh 2 vs. Mesh 1	**Mesh 3 vs. Mesh 2**	**Mesh 4 vs. Mesh 3**
Heat flux (%)	0.863	0.716	0.207
T at 1.98 m (%)	0.011	0.013	0.004
T RMS (%)	0.023	0.016	0.004

4.2. Mesh validation

The work of Sørensen et al. [44] was used to validate the present numerical results. The three turbulence models, each with two radiation models, provided six simulation results of the heat flux on the whole body and the velocity profile compared with the experimental data. In the study CFD, Tables 4.2 and 4.3 compare the measured and calculated heat flux and velocity field along the line above the head of the CTM.

Table 4.2: The comparison between simulated and experimental results

Body section	**Heat Flux**			**Deviation (%)**	
	Experiments (W/m^2)	Numerical study (W/m^2)	Current study (W/m^2)	Exp. vs Current study	Num. vs Current study
Foot	101.7	113.0	101.2	-0.5	-10
Leg	116.7	92.0	83.67	-28	-9
Thigh	98.8	87.8	86.3	-13	-2
Hand	101.2	97.0	96.95	-4	-0.05
Arm	99.1	91.5	84.93	-14	-7
Shoulder	85.9	82.7	104.9	22	27
Pelvis	90.5	88.1	95.6	6	9
Head	104.0	99.8	90.73	-13	-9
Chest	78.5	80.2	80.37	2	0.2
Back	76.9	82.4	92.95	21	13
Whole body	88.26	89.67	90.02	1.98	0.38

Table 4.2 shows the difference between the measured and calculated heat transfer when radiation and convection are combined. According to the Sørensen study [44], the estimated and measured total heat fluxes of the whole body generally agree excellently, with less than 10% deviations. The significant deviation in the leg, shoulder, and back regions can be explained by simplifying our CTM model and by the fact that the original human model differs in these regions.

Table 4.3: Mesh validation compared with three turbulence models and radiation models

	Turbulence models, including the radiation model						**Sørensen study** [44]
Parameters	k-ε		k-ω		SST		k-ε
	Discrete transfer	Monte Carlo	Discrete transfer	Monte Carlo	Discrete transfer	Monte Carlo	Surface-to-Surface
Heat flux $(\frac{W}{m^2})$	**64.99**	**63.19**	**89.86**	**87.93**	**89.58**	**90.01**	**88.26**
Velocity $(\frac{m}{s})$	**0.318**	**0.319**	**0.516**	**0.516**	**0.529**	**0.529**	**>0.5**
Error (%) on Heat flux	**26.4**	**28.4**	**1.8**	**0.37**	**1.51**	**1.99**	

All the compared results showed that the k-ω and SST turbulence models, either the Discrete Transfer or the Monte Carlo radiation model, agreed best with the heat flux and velocity measurements, as the error was less than 2%. However, the SST turbulence model was chosen because it combines k-ε and k-ω turbulence models as a blending function. In the near-wall zone, the SST model activates the k-ω model, while the rest of the flow is activated by the k-ε model [51]. The Monte Carlo method was used for the radiation model because it provides accurate and robust performance of the radiative heat transfer [53]. According to [54], the solution of this radiation model is commonly used as a benchmark for analyzing other radiation models' performance in an application involving complex geometry.

4.3. Case study

Since a benchmark simulation using CTM was validated adequately against experimental data, the next objective was to create and implement a space heating system. For this study, three case studies were evaluated regarding thermal comfort, and energy consumption was calculated for a comfortable environment for the occupants (Figure 4.4).

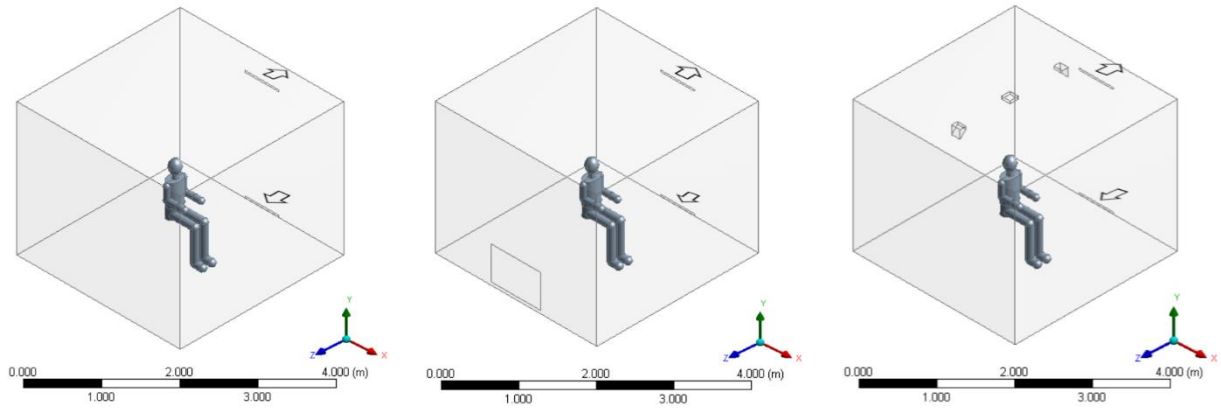

(a) Case 1 (b) Case 2 (c) Case 3

Figure 4.4: Geometry of case studies: a) forced heat convection; b) and c) forced heat convection and heat radiation

As can be seen in the figure above, Case 1 was simulated with a ventilation system only, and the positions and sizes of the supply and exhaust vents were placed in the corridor wall following the numerical studies mentioned earlier. In Case 2, a commercial radiator ($L\,(x) \times H(y) = 0.9\,m\, \times 0.6\,m$) was added to heat the space and placed on the exterior wall exposed to the outside temperature. In the numerical studies mentioned above, it has already been shown that placing the radiator near the cold area results in a more uniform temperature. Notice that Case 2 corresponds to a combination of forced heat convection and heat radiation. Finally, Case 3 demonstrates a new approach where the heating panels ($L\,(x) = H(y) = 0.1524\,m$) are placed on the ceiling to heat directly towards the occupant as a focused heating system. Notice that the third case corresponds to forced heat convection and heat radiation but is based on the focused panels.

4.4. Boundary settings

All three cases were conducted in winter conditions in Nur-Sultan, where the daily average temperature outside the room was -6.9°C, according to weather reports on the Internet [55]. The air velocity at the inlet was 0.15 m/s at a constant temperature of 21°C, according to the Interstate Council for Standardization, Metrology, and Certification (ISC) [56]. The interior walls, ceiling,

and floor were defined as adiabatic parameters, while the exterior wall was kept at -1°C as the temperature parameter. Different heat flux values were used for the radiator in Case 2 to meet the thermal comfort requirements. Similarly, in Case 3, a heat output was defined in the boundary settings for small heating panels.

Chapter 5 – Results and Discussion

In all three scenarios, simulations are used to determine the indoor air temperature and the mean radiant temperature to evaluate the thermal comfort for space heating. The results for each case are presented using temperature and velocity plots. A descriptive graph determines the thermal comfort indication by local thermal discomfort, PMV, and PPD values. Then, the energy consumption is given using the heat balance equation.

5.1. Temperature distribution in the domain

Figure 5.1 shows the distribution of the air temperature in the plane intersecting the region precisely in the center of the geometry of the occupant. It can thus be seen that the temperature contour correctly represents the temperature change around the occupant for each case.

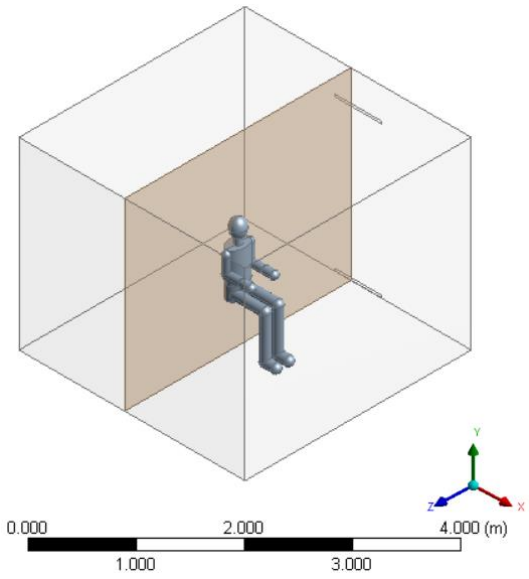

(a)

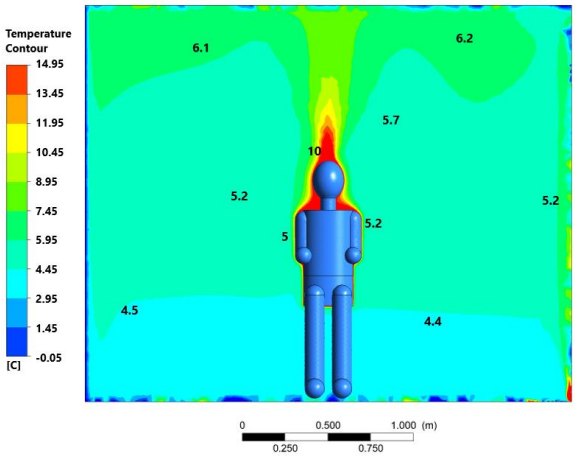

(b)

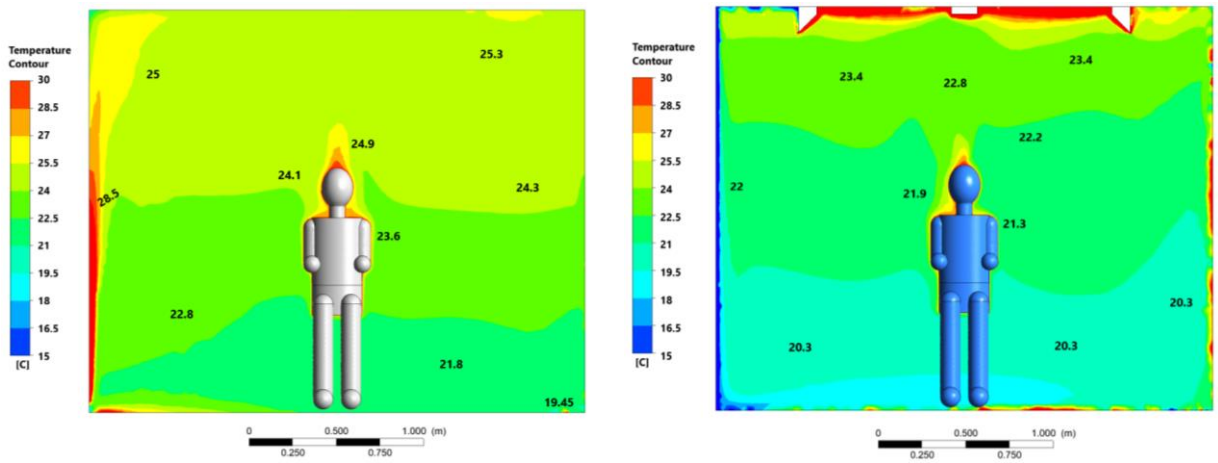

(c) (d)

Figure 5.1: Air temperature distribution along the x=1.38 m: a) the middle plane; b) Case 1; c) Case 2; d) Case 3

In case 1, the airflow comes from the right side of the occupant, and rises from below due to natural convection. As a result, the average temperature in the domain is 5.7°C, making the indoor environment cold under winter conditions (Figure 5.1, b). Therefore, adding a heating system and devices to the domain is necessary. For cases 2 and 3, heating panels with standard-sized commercial radiators were used. In these scenarios, the air temperature in the domain was 23.758°C and 22.678°C, respectively (Figure 5.1, c and d). These values are within the acceptable range according to ISO 7730 Standard [57].

5.2. Velocity field in the domain

In addition, the same plane intersecting the center of the occupant was used to contour the distribution of simulated velocity for comparison of each case (Figure 5.2). The airflow velocity was set to $0.15\ m/s$ direct into the area from the inlet.

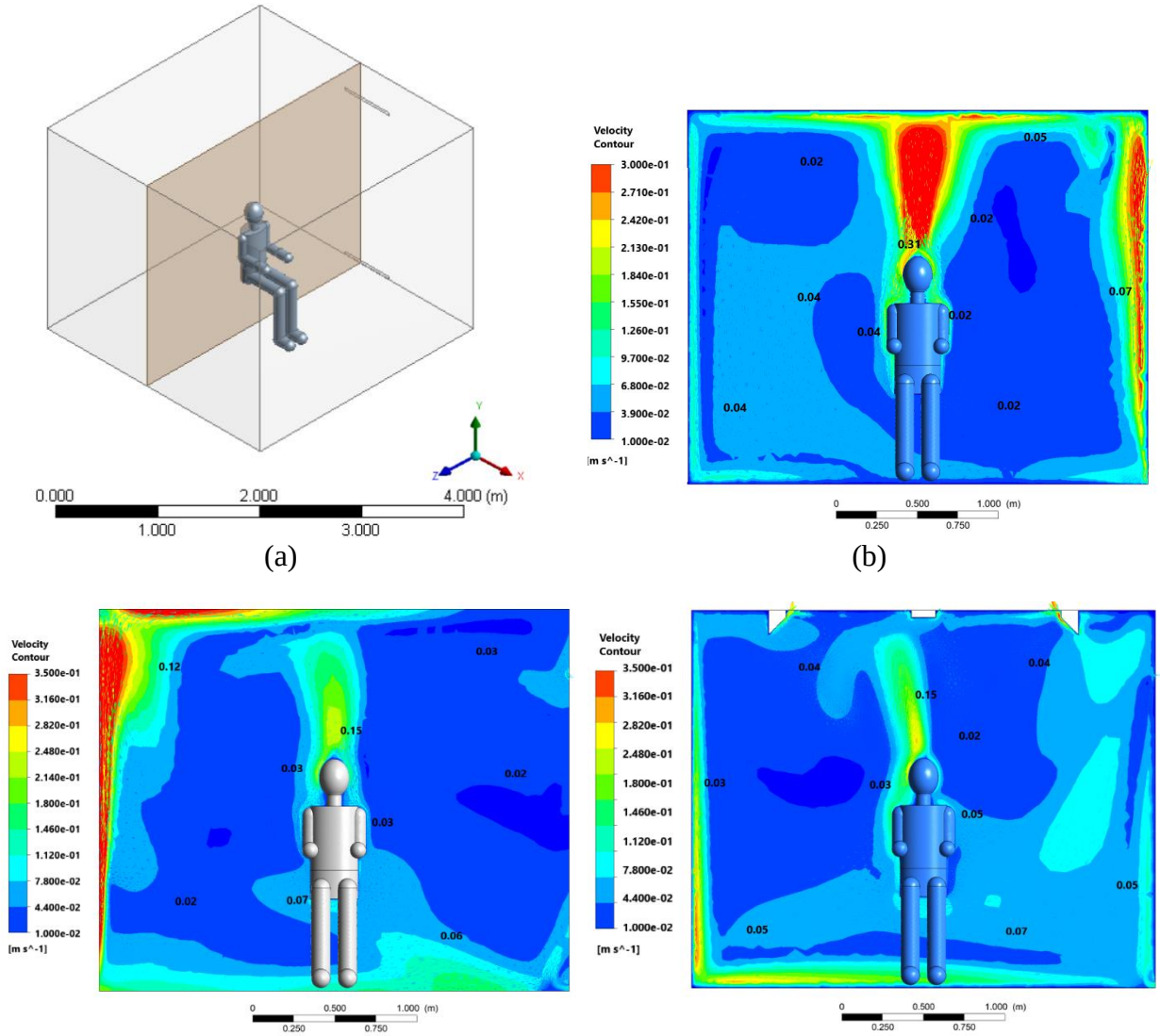

Figure 5.2: Air velocity distribution along the z=1.38 m: a) the middle plane; b) Case 1; c) Case 2; d) Case 3

To avoid discomfort, the mean air velocity in the occupied zone should be less than 0.15 m/s [57]. In Case 1, the air velocity increased from 0.01 m/s to 0.31 m/s as it rose from the ground. The velocity exceeded the limit for this case, as it was only a ventilated system with no heat sources (Figure 5.2, b). In the other cases, the air velocity did not exceed the limit and remained approximately below 0.15 m/s in the occupied zone (Figure 5.2, c and d).

5.3. Vertical temperature difference

According to thermal comfort standards [42] and [43], the vertical temperature difference between the head and ankle should not exceed 3°C. The graphs were constructed using other numerical studies that explain the vertical temperature difference [11, 58-59]. As shown in Figure 5.3, the temperature difference between the head and ankle regions is 4.15°C, 2.47°C, and 2.89°C, respectively. The area heated by the heat sources is within3°C, which shows that these cases achieve the acceptable comfort level and provide a comfortable environment for the occupant.

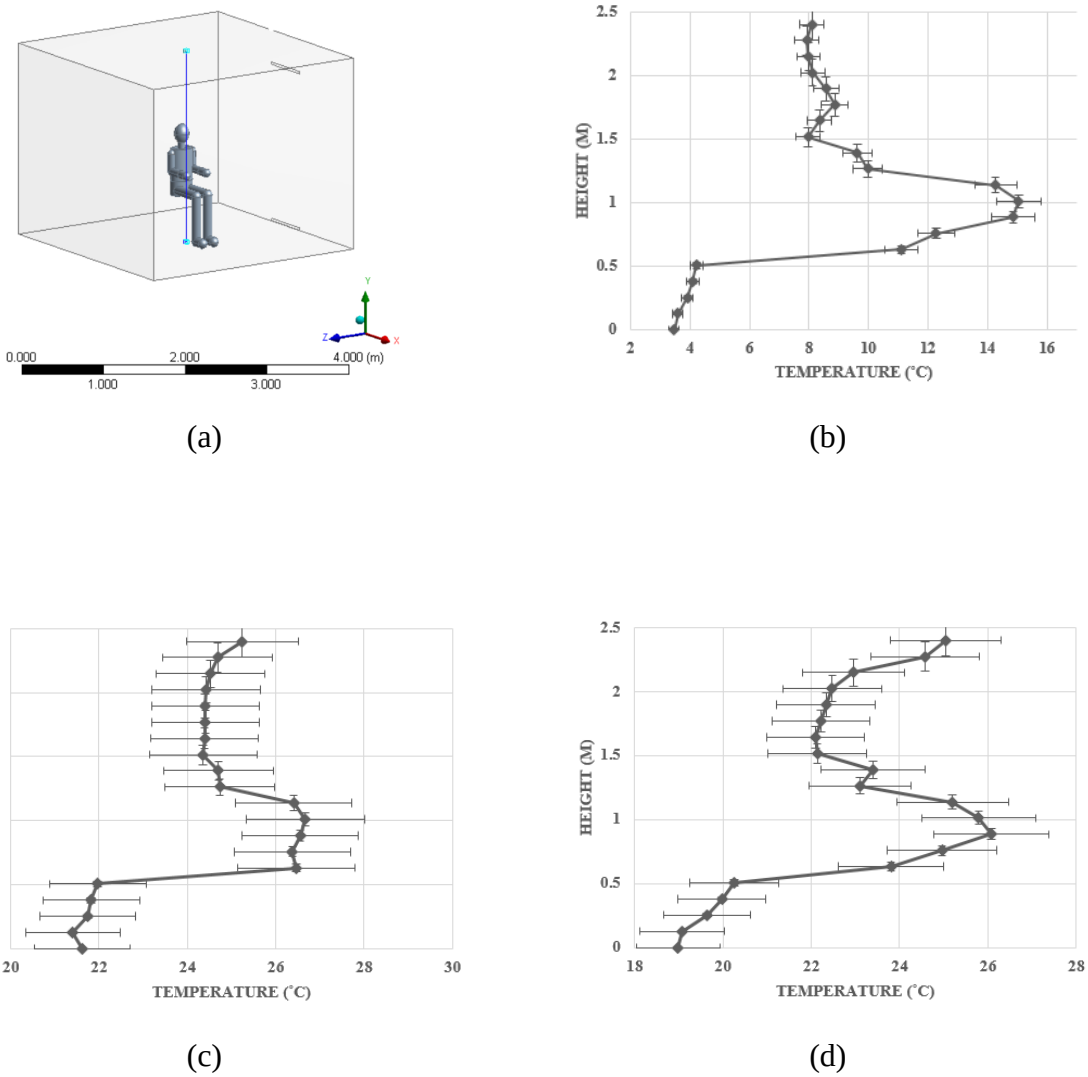

Figure 5.3: Vertical difference temperature results: a) center line; b) Case 1; c) Case 2; d) Case 3

5.4. Thermal comfort

It is essential to achieve acceptable thermal comfort using the PMV and PPD indices, as they are widely used in numerical studies that provide the actual values of comfort levels. This study used simulated air temperature and mean radiant temperature to evaluate PMV and PPD using an online PMV and PPD calculator following ASHRAE Standard 55-2017 [43]. The online tool is called the CBE Thermal Comfort Tool and was developed by the University of Berkeley [60]. We need to enter the air temperature and mean radiant temperature from the simulations and select other factors such as relative humidity, metabolic rate, and clothing degree. In these simulations, the sedentary occupant was predicted to wear casual winter clothing (*0.61 clo*) and be relaxed (*1 met*). The relative humidity value is recommended to be set to 50%, as this value is used in many numerical works. The CBE thermal comfort tool values were set for each case in PMV values of -7.43, -0.46, and -0.46, respectively (Figure 5.4). The result is whether the range is consistent with ASHRAE Standard 55-2020.

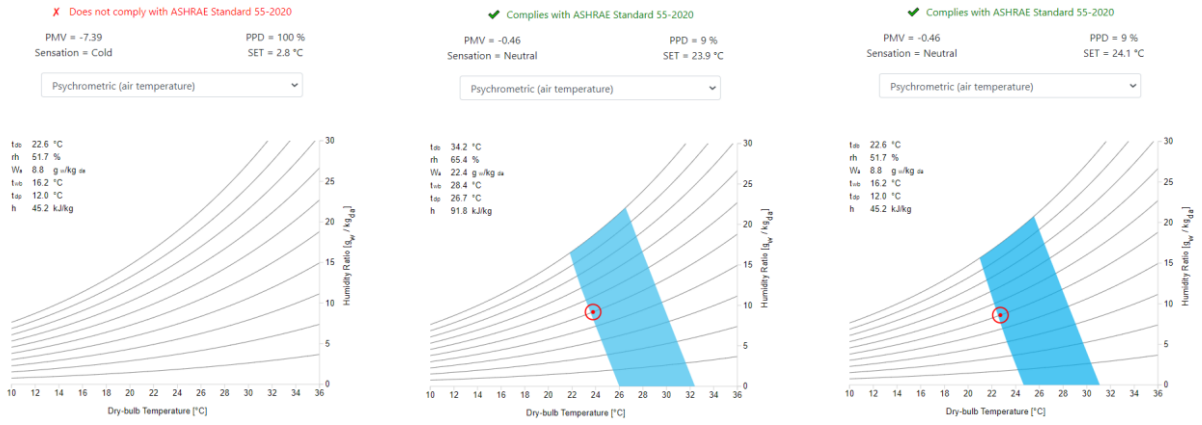

(a) (b) (c)

Figure 5.4: PMV and PPD values using CBE thermal comfort tool: a) Case 1; b) Case 2; c) Case 3

As shown in Figure 18, Case 1 did not meet ASHRAE Standard 55-2020, and the occupant was uncomfortable because he/she felt the cold in the space. The other two cases showed good acceptance of ASHRAE Standard 55-2020 by yielding a neutral feeling scale. Additionally, different PMV points on the plane were applied to the temperature contour to indicate PMV values at different locations in the area (Figure 5.5).

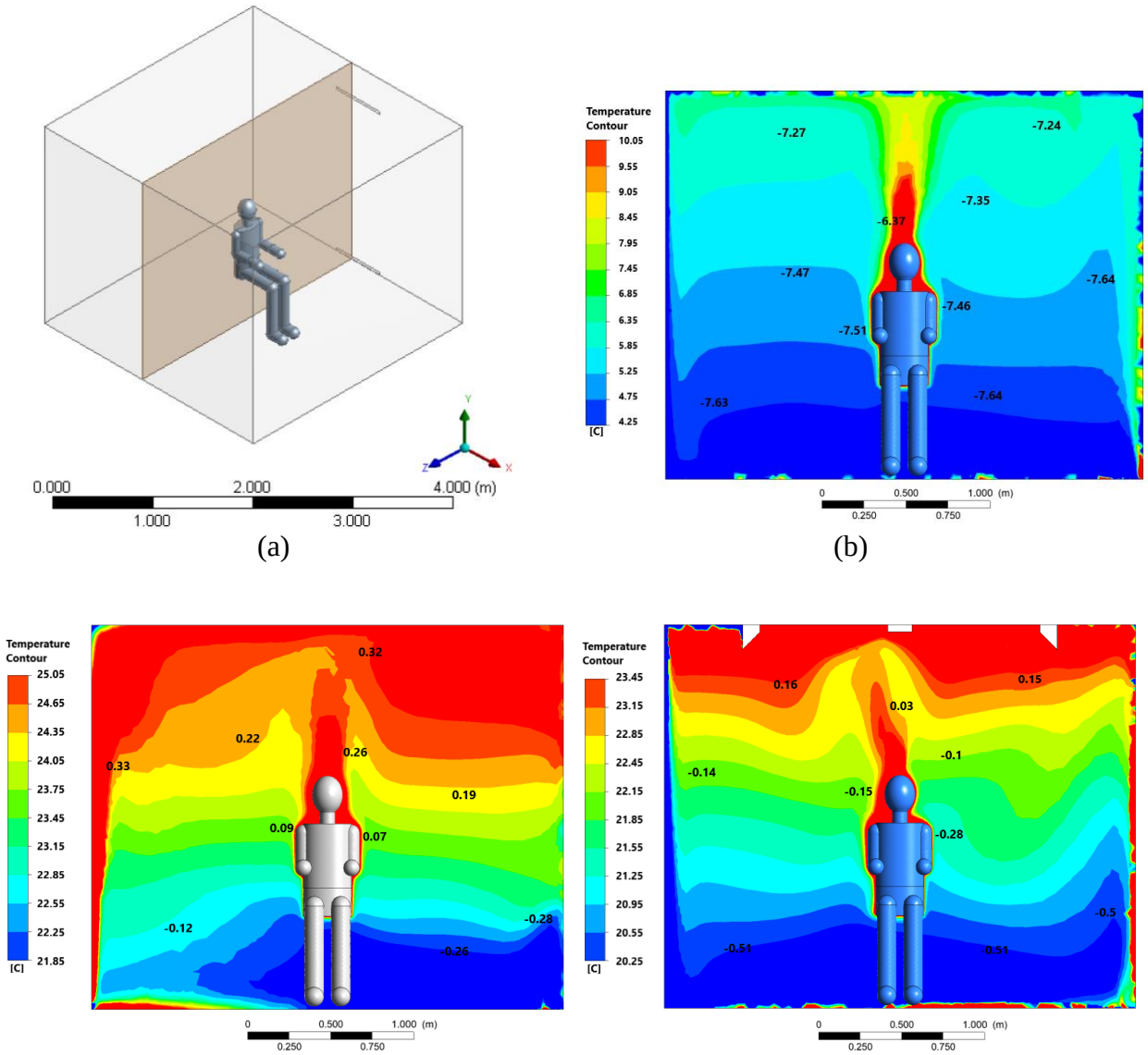

Figure 5.5: PMV comfort parameter along the plane at x=1.38m illustrated on air temperature profile: a) the middle plane; b) Case 1; c) Case 2; d) Case 3

Similarly, to represent the values of PPD at different locations in the area, various PPD points on the plane were applied to the temperature contour (Figure 5.6).

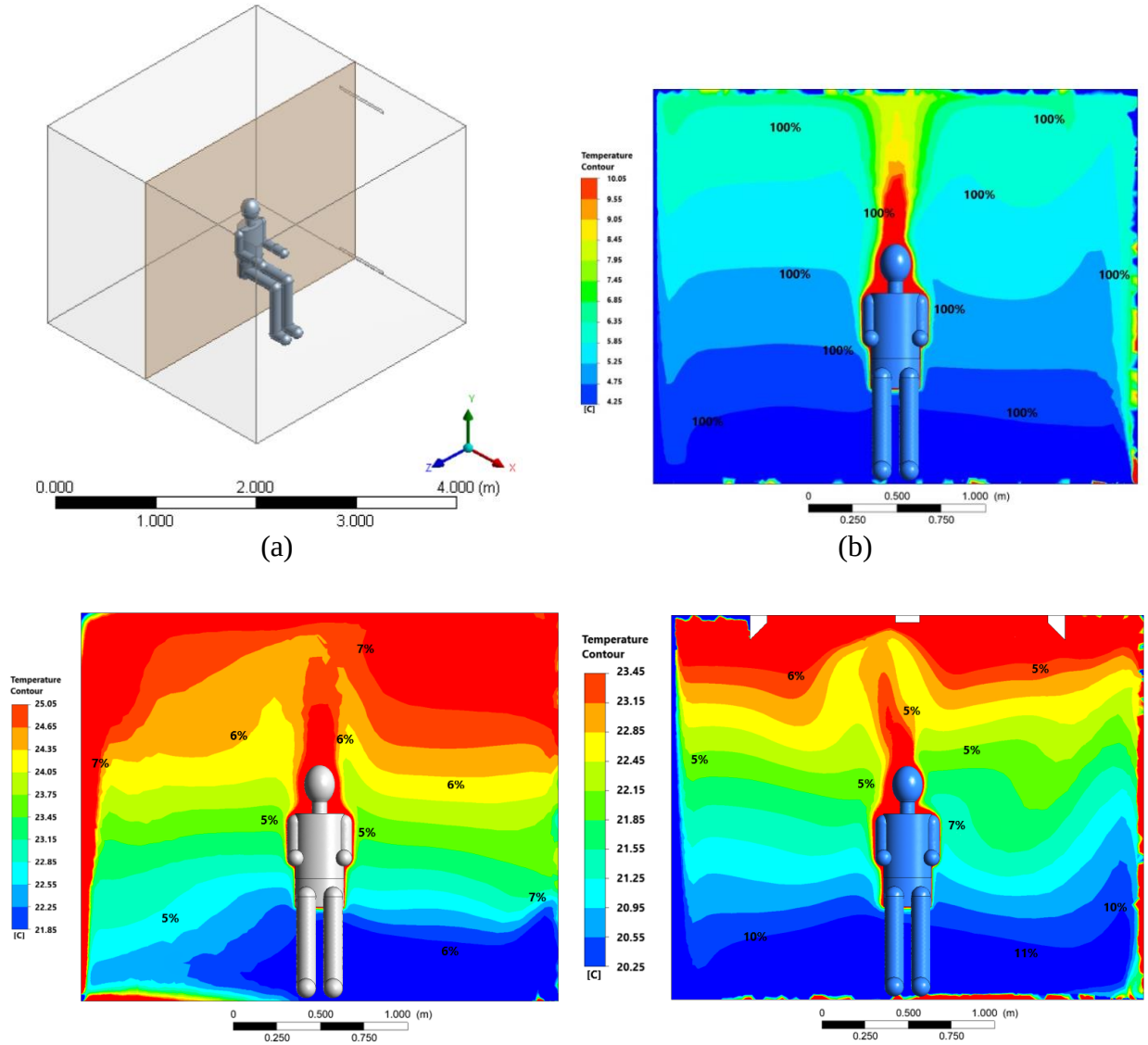

Figure 5.6: PPD comfort parameter along the plane at x=1.38m illustrated on air temperature profile: a) the middle plane; b) Case 1; c) Case 2; d) Case 3

5.5. Energy Consumption

The energy consumption for heating room evaluating by the following formula [61]:

$$\dot{Q} = \dot{Q}_R + \sum|\dot{m}_i \dot{h}_i| - \sum|\dot{m}_o \dot{h}_o| \quad (5.1)$$

where $\dot{m}_i$ is the mass flow at the inlet; $\dot{m}_o$ is the mass flow at the outlet; $\dot{h}_i$ is the static enthalpy at the inlet; $\dot{h}_o$ is the static enthalpy at the outlet; $\dot{Q}_R$ is the heat flux of radiator panel.

Since we have reached the thermal comfort level in the cases with the heating system in the range where the minimum accepted comfort level is, we next calculate the energy consumption required to compare the two cases. The calculation of the thermal power for the cases with heating panels is as follows:

- ***Case 2***

$$\dot{Q} = \dot{Q}_R + \sum|\dot{m}_i \dot{h}_i| - \sum|\dot{m}_o \dot{h}_o| \tag{5.2}$$

$$\dot{Q}_R = 2475.53\ \frac{W}{m^2} = 2475.53 \times 0.54 = 1\ 337\ [W]$$

The obtained values for equation: $\dot{m}_i = 8.7 \times 10^{-6}\ [\frac{kg}{s}]$; $\dot{m}_o = -4.14 \times 10^{-5}\ [\frac{kg}{s}]$; $\dot{h}_i = -3973\ [\frac{J}{kg}]$; $\dot{h}_o = -68.6\ [\frac{J}{kg}]$; $\dot{Q}_R = 1\ 351\ [W]$.

The amount of energy needed to heat the room is calculated by substituting the values obtained into equation (5.2):

$$\dot{Q} = 1\ 351 + |8.7 \times 10^{-6} \times (-3973)| - |(-4.14 \times 10^{-5}) \times (-68.6)| = 1\ 351\ [W]$$

$$\dot{Q} = 1\ 351\ [W] \approx 1.35\ kW$$

- ***Case 3***

$$\dot{Q} = \dot{Q}_{R1} + \dot{Q}_{R2} + \dot{Q}_{R3} + \sum|\dot{m}_i \dot{h}_i| - \sum|\dot{m}_o \dot{h}_o| \tag{5.3}$$

The obtained values for equation: $\dot{m}_i = 1.4 \times 10^{-5}\ [\frac{kg}{s}]$; $\dot{m}_o = -4.13 \times 10^{-5}\ [\frac{kg}{s}]$; $\dot{h}_i = -3948\ [\frac{J}{kg}]$; $\dot{h}_o = -2214\ [\frac{J}{kg}]$; $\dot{Q}_{R1} = 574.5\ [W]$; $\dot{Q}_{R2} = 232.9\ [W]$; $\dot{Q}_{R3} = 641\ [W]$.

The amount of energy needed to heat the room is calculated by substituting the values obtained into equation (5.3):

$$\dot{Q} = 574.5 + 232.9 + 641 + |1.4 \times 10^{-5} \times (-3948)| - |-4.13 \times 10^{-5} \times (-2214)|$$
$$= 574.5 + 232.9 + 641 + 0.06 - 0.09 = 1\,448\,[W]$$
$$\dot{Q} = 1\,448\,[W] \approx 1.45\,kW$$

The results showed that the energy required for case 2 was less than case 3, requiring about 1.35kW and 1.45kW respectively, to heat the domain under the same conditions. Thus, conventional heating is 6.9% more energy efficient than the proposed heating system. To explain why the proposed hating system might not work more efficiently. We need to consider that the presence of the ventilation adds a significant factor in removing or warming up since it is associated with forced heat convection, which is typically dominant over radiation heat transfer. A thorough study is pending to assess the role of radiation in comparison to convection. If the hypothesis is valid, a future study will focus on heating systems relying on natural convection and radiation only, such that the competitiveness of radiation focusing may be better appreciated.

Chapter 6 – Conclusions

In order to reduce the heating energy consumption in the residential sector, a focused heating system was proposed. A focused heating panel was assessed to heat an occupant directly in the room during winter compared to a traditional side radiator. Both base and proposed cases were provided with ventilation to support a parallel forced heat convection mechanism and air replacement. The proposed focused heating system was expected to perform similar or even better than the traditional heating system or energy saving. The numerical study was conducted using the CFD method in the ANSYS CFX software. The benchmark where an occupant is in an enclosed space was validated with the corresponding experimental data. A primary case with a pure ventilation system was also analyzed as benchmarking condition for both cases with combined forced convection and radiation. The most important criterion to be met was the occupant's thermal comfort. These are the results of the simulation:

- In case 1 (benchmark case), the PMV value was -7.43 and PPD was 100%, which means that the comfort in the room was not achieved unless the speed was taken above acceptable levels, and thus, the occupants had a cold sensation and were dissatisfied with the indoor environment. This is explained by the fact that there is no heating source under winter conditions, but just a stream of ventilated air at 21°C, which was not enough to warm the individual under comfortable conditions.
- In case 2, the performance of the traditional ventilation (at 21°C) with a side radiator heating system showed PMV and PPD values of -0.46 and 9%, respectively. Thus, the occupant felt neutral on the sensation scale, and thermal comfort was achieved. Heat output from the side radiator of about 1.35 kW was required to heat this room within the acceptable thermal comfort.
- In case 3, the ceiling's small, focused heating panels needed slightly more energy than a conventional heating system. However, thermal comfort was also achieved; the same values for PMV and PPD were -0.46 and 9%, respectively. The heat output difference between the conventional and the proposed heating system is 97 W.

In conclusion, the proposed idea can still be modified and optimized, but apparently, the forced heat convection attained by regular ventilation opaqued the potential benefits from the

focused radiators above the side radiator. Further work is necessary to assess mild or batch ventilation conditions, just for the air-change purpose. The heating happens by natural heat convection and radiation to explore a more precise scenario where the ventilation system does not mask the potential benefits of focused heating. On the other hand, this study has shown that the CFD method is a practical and valid tool suitable for heat transfer analysis in HVAC systems and can provide significant insight on heating and cooling systems considering their impact on the PMV and PPD parameters.

References

[1] Markov, D. (2002). Standards in thermal comfort. *Annual International Course: Ventilation and Indoor Climate, Sofia*, 147-157.

[2] The International Energy Agency (IEA), https://www.iea.org/

[3] Li, G., Kou, C., & Wang, H. (2019). Estimating city-level energy consumption of residential buildings: A life-cycle dynamic simulation model. *Journal of environmental management*, *240*, 451-462.

[4] ASHRAE (2016), HVAC Systems and Equipment. ASHRAE, Atlanta.

[5] Martinez, D., Ebenhack, B. W., & Wagner, T. (2019). *Energy efficiency: Concepts and calculations*. Elsevier.

[6] Yildiz, A., & Güngör, A. (2009). Energy and exergy analyses of space heating in buildings. *Applied Energy*, *86*(10), 1939-1948. (10), 1939-1948.

[7] Rhee, K. N., & Kim, K. W. (2015). A 50 year review of basic and applied research in radiant heating and cooling systems for the built environment. *Building and Environment*, *91*, 166-190.

[8] Calisir, T., Yazar, H. O., & Baskaya, S. (2017). Determination of the effects of different inlet-outlet locations and temperatures on PCCP panel radiator heat transfer and fluid flow characteristics. *International Journal of Thermal Sciences*, *121*, 322-335.

[9] Myhren, J. A., & Holmberg, S. (2009). Design considerations with ventilation-radiators: Comparisons to traditional two-panel radiators. *Energy and buildings*, *41*(1), 92-100.

[10] Sarbu, I., & Sebarchievici, C. (2015). A study of the performances of low-temperature heating systems. *Energy Efficiency*, *8*(3), 609-627.

[11] Hasan, A., Kurnitski, J., & Jokiranta, K. (2009). A combined low temperature water heating system consisting of radiators and floor heating. *Energy and Buildings*, *41*(5), 470-479.

[12] Ovchinnikov, P., Borodiņecs, A., & Strelets, K. (2017). Utilization potential of low temperature hydronic space heating systems: A comparative review. *Building and Environment*, *112*, 88-98.

[13] Olesen, B. W., & BW, O. (1980). Thermal comfort in a room heated by different methods.

[14] Hajdukiewicz, M., Geron, M., & Keane, M. M. (2013). Calibrated CFD simulation to evaluate thermal comfort in a highly-glazed naturally ventilated room. *Building and Environment*, *70*, 73-89.

[15] Wu, T., Clark, A. D., Mitchell, G. L., Lin, C. H., & Horstman, R. H. Application of CFD Predictions to Quantify Thermal Comfort for Indoor Environments.

[16] Dixit, A., & Gade, U. (2015). A case study on human bio-heat transfer and thermal comfort within CFD. *Building and Environment*, *94*, 122-130.

[17] Cao, Z., Niu, T., Sun, H., & Lu, X. (2020, August). A Simplified Method of Radiator to Improve the Simulation Speed of Room Temperature Distribution. In *International Symposium on Simulation and Process Modelling* (pp. 395-405). Springer, Singapore.

[18] Raczkowski, A., Suchorab, Z., & Brzyski, P. (2019). Computational fluid dynamics simulation of thermal comfort in naturally ventilated room. In *MATEC Web of Conferences* (Vol. 252, p. 04007). EDP Sciences.

[19] Risberg, D., Westerlund, L., & Hellström, G. J. (2017). Computational fluid dynamics simulation of indoor climate in low energy buildings: Computational set up. *Thermal Science*, *21*(5), 1985-1998.

[20] Teodosiu, C., Kuznik, F., & Teodosiu, R. (2014). CFD modeling of buoyancy driven cavities with internal heat source—Application to heated rooms. *Energy and Buildings*, *68*, 403-411.
[21] Embaye, M., Al-Dadah, R. K., & Mahmoud, S. (2016). Numerical evaluation of indoor thermal comfort and energy saving by operating the heating panel radiator at different flow strategies. *Energy and Buildings*, *121*, 298-308.
[22] Horikiri, K., Yao, Y., & Yao, J. (2015). Numerical optimisation of thermal comfort improvement for indoor environment with occupants and furniture. *Energy and Buildings*, *88*, 303-315.
[23] Gendelis, S., & Jakovičs, A. (2010). Numerical modelling of airflow and temperature distribution in a living room with different heat exchange conditions. *Latvian journal of physics and technical sciences*, *47*(4), 27-43.
[24] Myhren, J. A., & Holmberg, S. (2008). Flow patterns and thermal comfort in a room with panel, floor and wall heating. *Energy and buildings*, *40*(4), 524-536.
[25] Bohojło, A. (2011). Numerical Analysis of Thermal Comfort Parameters in Living Quarters. *acta mechanica et automatica*, *5*, 5-10.
[26] Sevilgen, G., & Kilic, M. (2011). Numerical analysis of air flow, heat transfer, moisture transport and thermal comfort in a room heated by two-panel radiators. *Energy and buildings*, *43*(1), 137-146.
[27] Horikiri, K., Yao, Y., & Yao, J. (2014). Modelling conjugate flow and heat transfer in a ventilated room for indoor thermal comfort assessment. *Building and Environment*, *77*, 135-147.
[28] Errebai, F. B., Derradji, L., & Amara, M. (2017). Thermal behaviour of a dwelling heated by different heating systems. *Energy Procedia*, *107*, 144-149.
[29] Raczkowski, A., Suchorab, Z., Połednik, B., Zarzeka-Raczkowska, E., & Życzyńska, A. (2018, July). Computational fluid dynamics simulation of thermal comfort in naturally ventilated room by the fresh air valve installed in an external wall. In *AIP Conference Proceedings* (Vol. 1988, No. 1, p. 020041). AIP Publishing LLC.
[30] Rabanillo-Herrero, M., Padilla-Marcos, M. Á., Feijó-Muñoz, J., & Meiss, A. (2019). Effects of the radiant heating system location on both the airflow and ventilation efficiency in a room. *Indoor and Built Environment*, *28*(3), 372-383.
[31] Karacavus, B., & Aydin, K. (2019). Numerical investigation of general and local thermal comfort of an office equipped with radiant panels. *Indoor and Built Environment*, *28*(6), 806-824.
[32] Khalil, E. E., & Sobhi, M. (2020). Air Flow Patterns and Thermal Comfort in a Room with Diverse Heating Systems. In *AIAA Scitech 2020 Forum* (p. 1221).
[33] Maher, D., Hana, A., & Sammouda, H. (2020). Numerical approximation of air flow, temperature distribution and thermal comfort in buildings. *Scientific African*, *8*, e00353.
[34] Anthony, A. S., & Verma, T. N. (2021). NUMERICAL ANALYSIS OF NATURAL CONVECTION IN A HEATED ROOM AND ITS IMPLICATION ON THERMAL COMFORT. *Journal of Thermal Engineering*, *7*(1), 37-53.
[35] Yan, Y., Li, X., Yang, L., & Tu, J. (2016). Evaluation of manikin simplification methods for CFD simulations in occupied indoor environments. *Energy and Buildings*, *127*, 611-626.
[36] Miyanaga, T., Urabe, W., & Nakano, Y. (2001). Simplified human body model for evaluating thermal radiant environment in a radiant cooled space. *Building and Environment*, *36*(7), 801-808.

[37] Cropper, P. C., Yang, T., Cook, M. J., Fiala, D., & Yousaf, R. (2009, July). Simulating the effect of complex indoor environmental conditions on human thermal comfort. In *Building Simulation '09, 11th Internat. IBPSA Conference, Glasgow, Proc. 1367-1373*.
[38] Gao, N. P., Zhang, H., & Niu, J. L. (2007). Investigating indoor air quality and thermal comfort using a numerical thermal manikin. *Indoor and built environment*, *16*(1), 7-17.
[39] Nielsen, P. V., Murakami, S., Kato, S., Topp, C., & Yang, J. H. (2003). Benchmark tests for a computer simulated person. *Aalborg University, Indoor Environmental Engineering*.
[40] Nielsen, Peter V., Shuzo Murakami, Shinsuke Kato, Claus Topp, and Jeong-Hoon Yang. "Benchmark tests for a computer simulated person." *Aalborg University, Indoor Environmental Engineering* (2003).
[41] Nilsson, H. O., Brohus, H., & Nielsen, P. V. (2007). CFD modeling of thermal manikin heat loss in a comfort evaluation benchmark test. In *Proceedings of Roomvent 2007: Helsinki 13-15 June 2007*. FINVAC ry.
[42] AC08024865, A. (Ed.). (2005). *Ergonomics of the thermal environment-Analytical determination and interpretation of thermal comfort using calculation of the PMV and PPD indices and local thermal comfort criteria*. ISO.
[43] ANSI/ASHRAE (2017) Standard 55: 2017, Thermal Environmental Conditions for Human Occupancy. ASHRAE, Atlanta.
[44] Sørensen, D. N., & Voigt, L. K. (2003). Modelling flow and heat transfer around a seated human body by computational fluid dynamics. *Building and environment*, *38*(6), 753-762.
[45] *Ansys® Academic Research Mechanical, Release 19.2, Help System, Coupled Field Analysis Guide, ANSYS, Inc.*
[46] Wendt, J. F. (Ed.). (2008). *Computational fluid dynamics: an introduction*. Springer Science & Business Media.
[47] Lopez-Ruiz, R. (Ed.). (2016). *Numerical Simulation: From Brain Imaging to Turbulent Flows*. BoD–Books on Demand.
[48] Bardina, J. E., Huang, P. G., & Coakley, T. J. (1997). Turbulence modeling validation, testing, and development.
[49] ANSYS CFX-Solver Theory Guide (2011)
[50] Karabay, H., Arıcı, M., & Sandık, M. (2013). A numerical investigation of fluid flow and heat transfer inside a room for floor heating and wall heating systems. *Energy and Buildings*, *67*, 471-478.
[51] Stamou, A., & Katsiris, I. (2006). Verification of a CFD model for indoor airflow and heat transfer. *Building and Environment*, *41*(9), 1171-1181.
[52] Alsaad, H., & Voelker, C. (2020). Performance evaluation of ductless personalized ventilation in comparison with desk fans using numerical simulations. *Indoor air*, *30*(4), 776-789.
[53] Malalasekera, W., Versteeg, H. K., Henson, J. C., & Jones, J. C. (2002). Calculation of radiative heat transfer in combustion systems. *Clean Air*, *3*(1), 113-143.
[54] Parthasarathy, G., Patankar, S. V., Chai, J. C., & Lee, H. S. (1995). Monte Carlo solutions for radiative heat transfer in irregular two-dimensional geometries. *Journal of heat transfer*, *117*(3), 792-794.
[55] https://www.accuweather.com/
[56] Interstate Council for Standardization, Metrology and Certification (ISC) BI Group
[57] ISO EN 7730:1994, Moderate Thermal Environments—Determination of the PMV and PPD Indices and Specification of the Conditions for Thermal Comfort, revised version, International Organization for Standardization, Geneva, 1994.

[58] Le Dréau, J., Heiselberg, P., & Jensen, R. L. (2015, February). A full-scale experimental set-up for assessing the energy performance of radiant wall and active chilled beam for cooling buildings. In *Building Simulation* (Vol. 8, No. 1, pp. 39-50). Tsinghua University Press.
[59] Peng, P., Gong, G., Deng, X., Liang, C., & Li, W. (2020). Field study and numerical investigation on heating performance of air carrying energy radiant air-conditioning system in an office. *Energy and Buildings*, *209*, 109712.
[60] https://comfort.cbe.berkeley.edu/
[61] Aryal, P., & Leephakpreeda, T. (2015). CFD analysis on thermal comfort and energy consumption effected by partitions in air-conditioned building. Energy Procedia, 79, 183-188.

Appendices

Table 1. An optimal and acceptable ranges for variables in a residential buildings by BI Group construction [55].

Season	Types of room	Air temperature (℃)		Mean radiant temperature (℃)		Relative Humidity (%)		Air speed (m/s)	
		optimal	acceptable	optimal	acceptable	optimal	Acceptable (and less than 60)	Optimal (and less than 60)	Acceptable (and less than 60)
Winter	Living room	**20-22**	**18-24 (20-24)**	**19-20**	**17-23 (19-23)**	**45-30**	**60**	**0.15**	**0.2**
	Living room (outside temperature - 31℃ and below)	**21-23**	**20-24 (22-24)**	**20-22**	**19-23 (21-23)**	**45-30**	**60**	**0.15**	**0.2**
	Study room (workplace; relaxation room)	**20-22**	**18-24**	**19-21**	**17-23**	**45-30**	**60**	**0.15**	**0.2**
Summer	Living room	**22-25**	**20-28**	**22-24**	**18-27**	**60-30**	**65**	**0.2**	**0.3**